

Detection of Pancreatic Adenocarcinoma *in vivo* with S100A9 Liposomes

Tess V. Dupre¹, Christopher England¹, Justin Huang², Lacey R. McNally^{1,2}

¹Department of Pharmacology and Toxicology, University of Louisville, Louisville, KY

²Department of Medicine, University of Louisville, Louisville, KY

ABSTRACT

Purpose: Delivering effective drugs at effective concentrations to all cells in solid tumors, especially pancreatic adenocarcinoma, remains challenging due to low drug accumulation within tumors and high levels of systemic toxicity. To overcome these problems, S100A9 liposomes can be utilized to enhance drug delivery. We hypothesize that S100A9 liposomes will exhibit enhanced accumulation in pancreatic orthotopic tumors due to S100A9 specificity for the EMMPRIN receptor.

Methods: Pancreatic cell lines, S2VP10, MiaPaCa2, S2CP9, and Panc-1, were evaluated for EMMPRIN expression along with ES2 (positive control) and MCF7 (negative control) using western blot. Liposomes were bioconjugated with S100A9 and CF750 NIR dye. Specificity and activity of the S100A9 liposomes were studied using flow-cytometry. SCID mice were orthotopically implanted with S2VP10 cells. After tumors reached 3mm, 200 μ L of 5 OD S100A9 liposomes was IV injected into mice. Mice were imaged using 2D AMI imaging and 3D MSOT.

Results: EMMPRIN expression was seen at 1.2X and 0.9X relative abundance in S2VP10 and MiaPaCa-2 cells respectively; however, MCF7 expressed 0.1X relative abundance EMMPRIN. Flow-cytometry showed cellular uptake of S100A9 liposomes in S2VP10 and MiaPaCa2 cells at ~92% and ~84% respectively. 3D MSOT imaging and 2D AMI imaging showed accumulation of the S100A9 liposomes at the tumor.

Conclusion: The S100A9 liposome selectively targeted pancreatic orthotopic tumors *in vivo*, thus establishing that the stealth liposomes can be used as a drug delivery system for an alternative pancreatic cancer treatment.

MATERIALS & METHODS

Pancreatic cancer cell lines MiaPaca2 and S2VP10 were utilized in this study along with MCF-7 and ES2 cell lines, a breast cancer and ovarian cancer cell line, respectively. MiaPaca-2 and MCF7 cells were grown in DMEM with 10% FBS and 1% L-Glutamine while S2VP10 and ES2 cells were grown in RPMI 1640 with 10% FBS and 1% L-Glutamine at 37°C. Western Blot analysis of EMMPRIN expression was used on S2VP10, MiaPaCa-2, Panc-1, S2CP9, ES2, and MCF-7 cell lines. MCF7, ES2, S2VP10, MiaPaCa2 were used for flow cytometry to ensure active binding of receptor. Immunocytochemistry was performed on S2VP10, ES2, and MCF 7. Cells were incubated with CF-750 dye alone, bioconjugated S100A9 probe, naked liposome, and S100A9 targeted liposome for 1-h; scraped and collected for flow cytometry. SCID mice were orthotopically implanted with S2VP10 cells. Tumor growth was monitored using 2D AMI imaging. After tumors reached 3mm, 200 μ L of 5 OD S100A9 liposomes was IV injected into mice. Accumulation and biodistribution of the probe was monitored with AMI imaging.

RESULTS

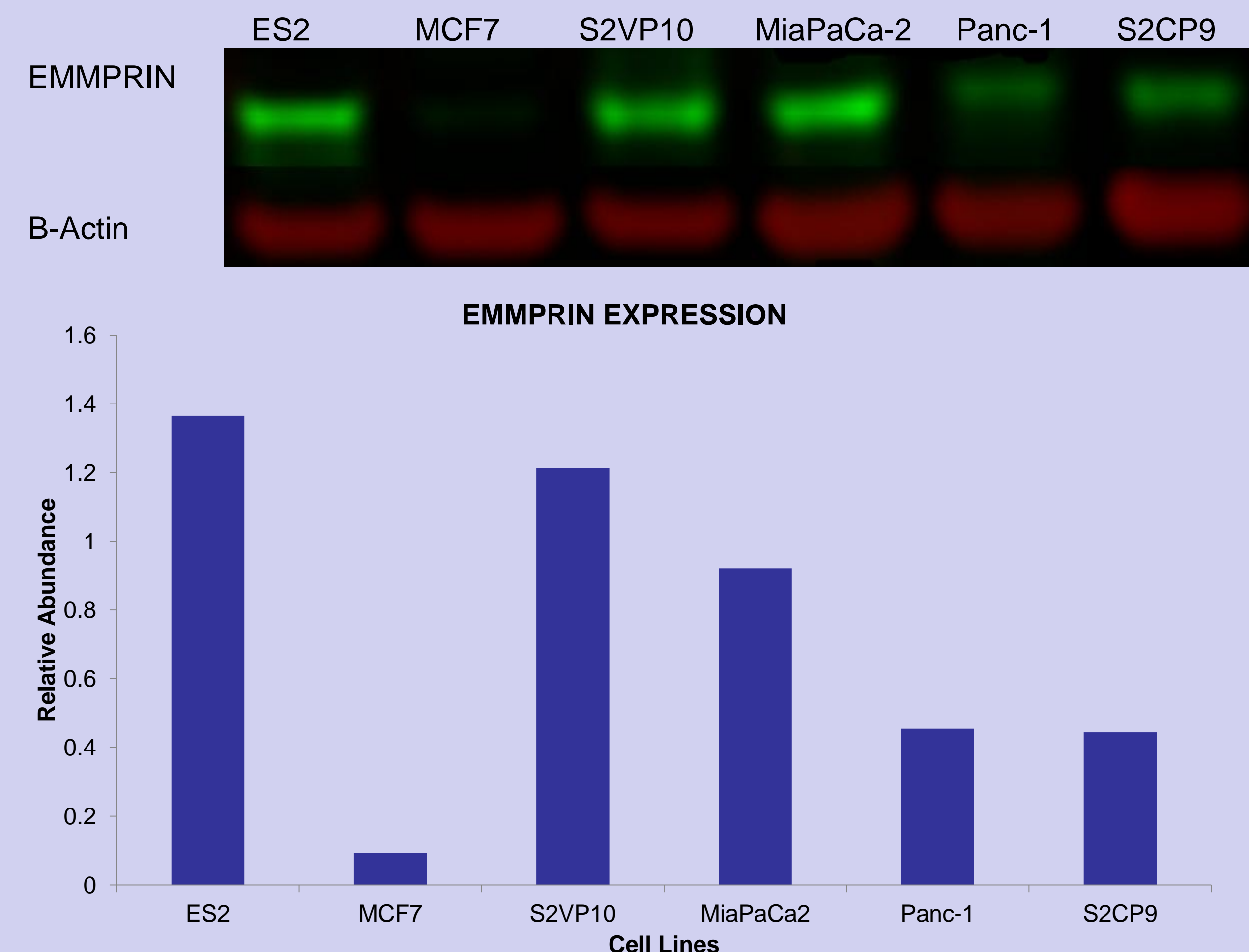


Figure 1: (top) Western blot image of EMMPRIN Expression. (bottom) Dose symmetry of EMMPRIN Expression in pancreatic cell lines and positive and negative controls with respect to actin. EMMPRIN expression was seen at 1.2X and 0.9X relative abundance in S2VP10 and MiaPaCa-2 cells respectively; however, MCF7 expressed 0.1X relative abundance EMMPRIN.

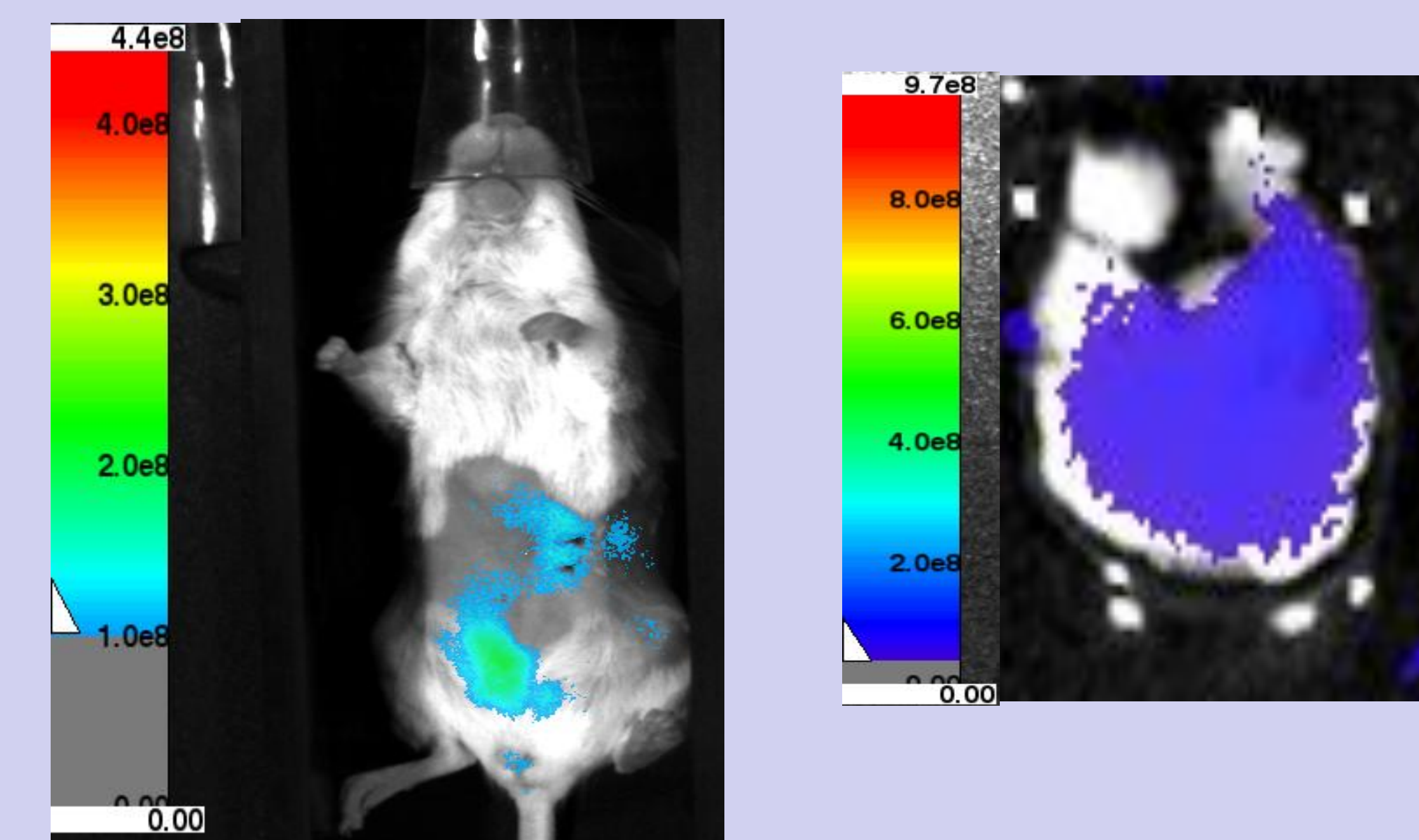


Figure 4: Accumulation of the S100A9 liposomes was observed at the 6hr time point using 2D AMI imaging. S2VP10 cells were orthotopically injected into mice. After tumors were palpable, S100A9 probe was injected to identify pancreatic tumors. Probe accumulated within tumors at 6hr post injection. A representative mouse (Right) demonstrates preferential binding. Probe accumulation in pancreas was confirmed ex vivo (Left).

CONCLUSION

EMMPRIN was found to be overexpressed in pancreatic cancer cell lines, making it a prime candidate for active targeting. The evaluation of Pancreatic. S100A9 liposomes showed an increased affinity for pancreatic cancer cell lines S2VP10 and MiaPaCa2. Accumulation of the liposomes observed via AMI imaging elucidates that S100A9 liposomes selectively targeted the pancreatic orthotopic tumor and has potential to be used as a delivery system for alternative pancreatic cancer treatment.

FUTURE DIRECTIONS

Pancreatic cancer cells are addicted to autophagy, thus using the metabolic process as a survival mechanism. We believe that utilizing the S100A9 liposomes as a drug delivery system for chloroquine, an autophagy inhibitor, will decrease systemic drug toxicity and increase pharmacological drug efficacy and potency.

ACKNOWLEDGEMENTS

This work was supported by CA139050 and R25- CA-134283 from the National Cancer Institute

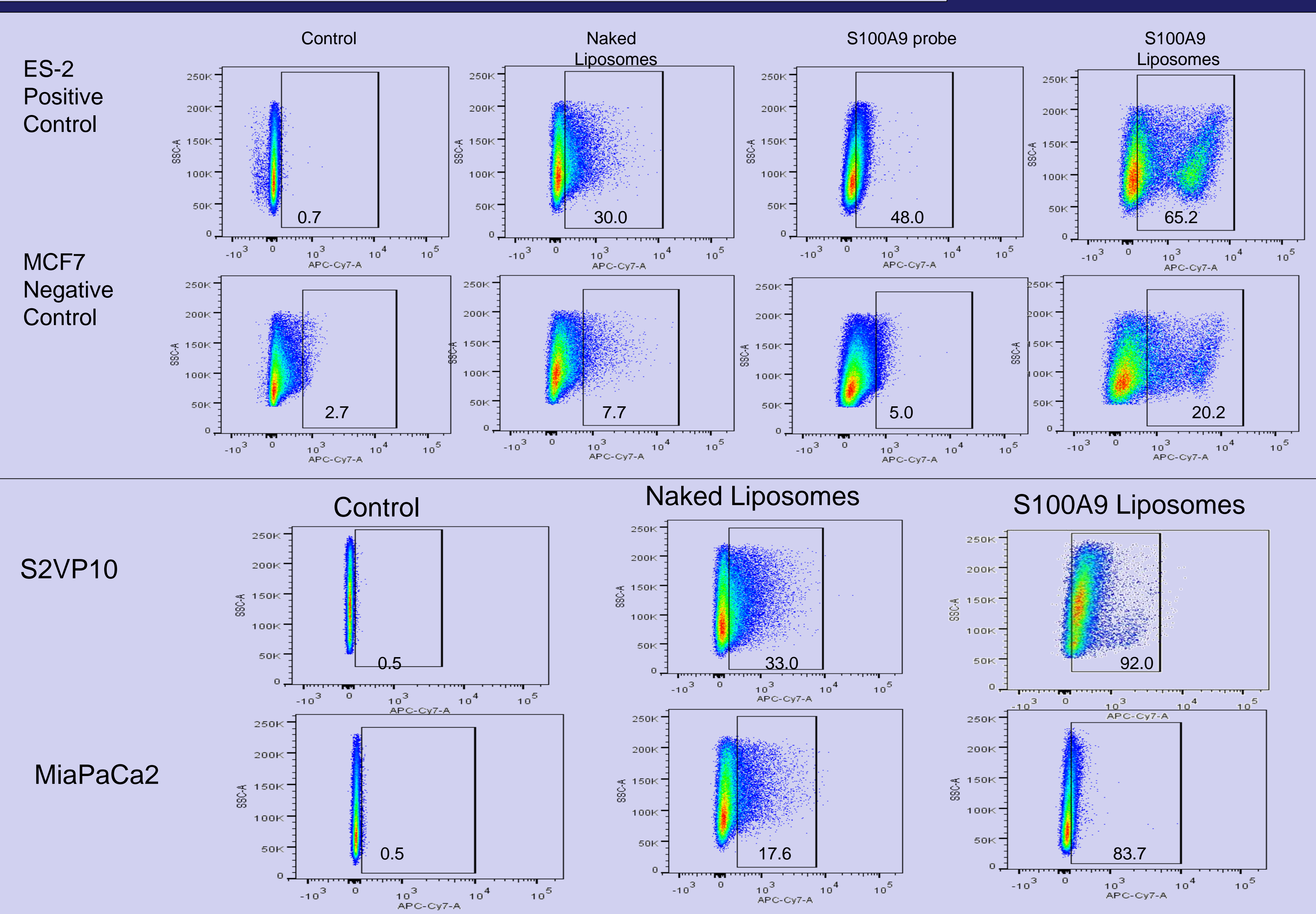


Figure 2: Flow Cytometry was performed on positive control ES2 (ovarian cancer), negative control MCF7 (breast cancer), and pancreatic cancer lines S2VP10, and MiaPaca-2 to test the activity of the S100A9 targeted liposomes, ~92% and ~84% binding was seen in S2VP10 and MiaPaCa2 Cells respectively.

Differential Expression of Chemokine Receptors in Lung Cancer Metastasis

Taylor N. Hermann, Rajesh K. Sharma, Zinal S. Chheda, and Bodduluri Haribabu.

James Graham Brown Cancer Center, School of Medicine, University of Louisville, Louisville, KY 40202



Abstract

Lung cancer is the leading cause of cancer related deaths in the United States. Lack of early diagnosis, metastasis, and resistance to treatments are major causes of the poor survival rate of lung cancer patients. Metastasis, the spread of cancer cells from the primary tumor to other non-adjacent organs, accounts for most of the cancer related deaths. The commonly used metastasis models utilize intravenous injection of tumor cells, thus bypassing the egression of malignant cells an obligatory step in metastasis of spontaneous cancers. We developed a unique metastasis model by *in vivo* passaging the Lewis lung carcinoma (3LL) cells and maintaining them *in vivo* with 7-11 days of intermittent culture in between passages. When injected subcutaneously (s.c.), parental 3LL cells have minimal metastasis, while *in vivo* passaged 3LL cells (p-3LL) show robust metastasis. Chemokine receptors on cancer enable the cancer cells to metastasize to other areas in the body. Given the paramount importance of chemokine signaling and receptors in cancer metastasis, we decided to study the expression profile of every chemokine receptor. This was done in order to study the chemokine receptors which may play the most important roles in 3LL metastasis in mice. Real-time PCR was used to examine the transcript levels of every chemokine receptors in 3LL and p-3LL cells and tumors. CCR6 and CXCR7 were found to be up-regulated in the passage tumors compared to the parental tumors, possibly indicating these receptors play a pro-metastatic role in cancer cells. CCR1 and CCR3 were down-regulated in the tumors, possibly indicating these receptors either play an anti-metastatic role or play no role whatsoever. The chemokine receptors CCR3, CCR4, CCR9, and CXCR4 were up-regulated in the p-3LL cells as compared to the 3LL cells, indicating that these receptors may play an important role in promoting lung cancer metastasis. The chemokine receptors CCR1, CCR6, CXCR1, CXCR7, CX3CR1, and BLT1 all showed a significant reduction in the p-3LL cells. This down-regulation may mean these chemokine receptors do not play a role in the increase in metastasis of the p-3LL cells or may play an anti-metastatic role. Each of the other chemokine receptors demonstrated no significant transcript level change in the passage cells compared to the parental cells, suggesting these receptors do not play a role in metastasis.

Models of Experimental and Spontaneous Metastasis

The widespread use of experimental metastasis models refers to the injection of tumor cells directly to the systemic circulation where site of injection largely defines the metastatic site. For example i.v. to lungs; hepatic vein to liver; heart to bones and so on.

The most common site of tumor cell injection employed is the lateral tail vein in mice which primarily results in pulmonary metastases in variety of the implantable models studied.

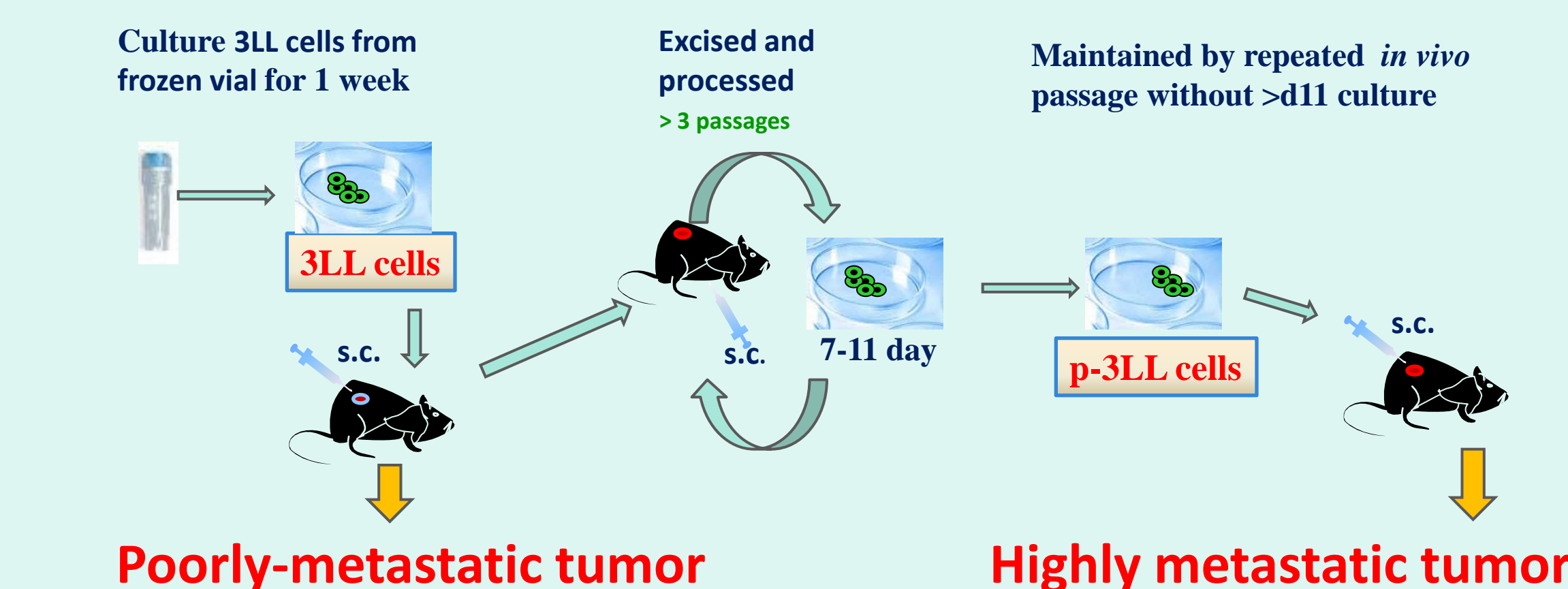
The fact that the early steps in the metastatic cascade are eliminated through experimental metastasis modeling is a potential disadvantage.

Furthermore, the process of spontaneous metastasis from a primary site may be associated with selection events that yield a distinct profile of successful metastasis.

Given the concerns about the relevance of experimental metastasis, it is important to develop spontaneous metastasis models relevant for delineation of molecular events taking place during metastasis in cancer patients.

Spontaneous Metastasis Model

Fig.1: Generation and maintenance of poorly (3LL) vs. highly metastatic (p-3LL) line:



Poorly-metastatic tumor

Highly metastatic tumor

Fig. 2: 3LL cells show minimal metastasis, while p-3LL cells show robust metastasis in subcutaneous model of spontaneous metastasis.

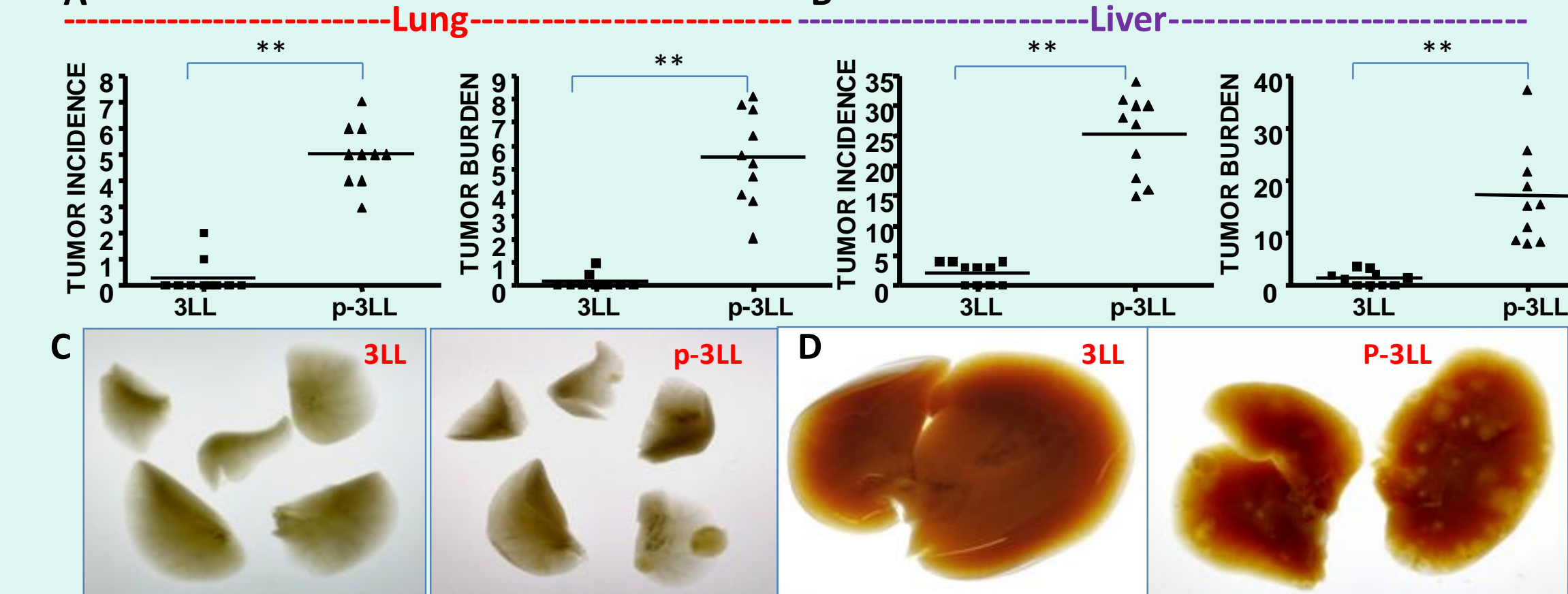
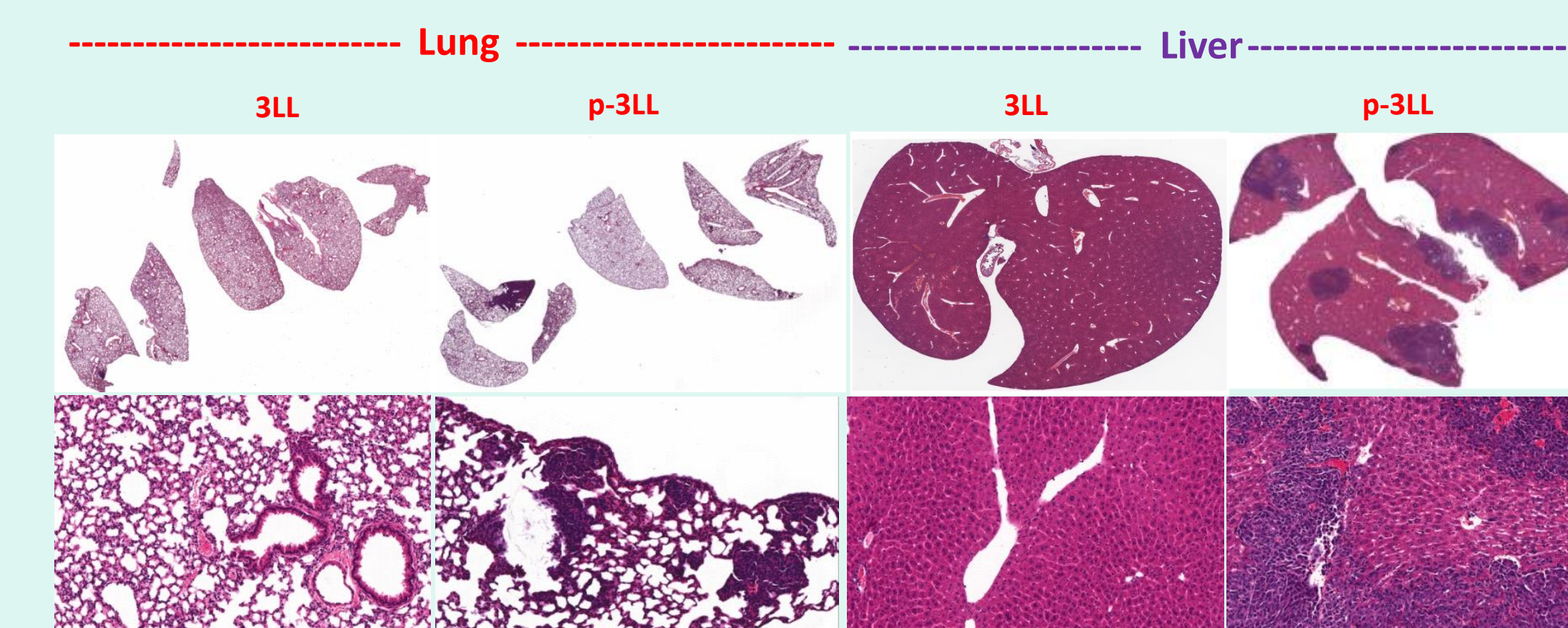


Fig 3: H&E histopathology for the lungs and livers from spontaneous metastasis shown in Fig. 2.



Role of chemokines and chemokine receptors

Chemokines are proteins discharged by cells. They cause the activation and accumulation of leukocytes from bloodstream to a site of infection/inflammation
 Chemokine receptors are expressed on different types of leukocytes. Some are always expressed but others are expressed only when induced
 The majority of cells are able to secrete chemokines provided the right stimulus
 Some chemokines have been found to inhibit tumor growth and angiogenesis while others have been found to promote these cancer spreading processes. These roles of chemokines are still being studied
 Chemokines may increase the body's counterattacks to infection, tumors and vaccines

CC and CXC chemokine receptors and their ligands

Receptor	Chemokine Ligands
CCR1	CCL1 (MIP-1α), CCL2 (MIP-1β), CCL3 (MIP-1γ), CCL4 (MIP-1δ), CCL5 (MIP-1β), CCL6 (MIP-1γ), CCL7 (MIP-1α), CCL8 (MIP-1β), CCL9 (MIP-1γ), CCL10 (MIP-1α), CCL11 (MIP-1β), CCL12 (MIP-1γ), CCL13 (MIP-1α), CCL14 (MIP-1β), CCL15 (MIP-1γ), CCL16 (MIP-1α), CCL17 (MIP-1β), CCL18 (MIP-1γ), CCL19 (MIP-1α), CCL20 (MIP-1β), CCL21 (MIP-1γ), CCL22 (MIP-1α), CCL23 (MIP-1β), CCL24 (MIP-1γ), CCL25 (MIP-1α), CCL26 (MIP-1β), CCL27 (MIP-1γ), CCL28 (MIP-1α), CCL29 (MIP-1β), CCL30 (MIP-1γ)
CCR2	CCL2 (MIP-1β), CCL3 (MIP-1γ), CCL4 (MIP-1δ), CCL5 (MIP-1β), CCL6 (MIP-1γ), CCL7 (MIP-1α), CCL8 (MIP-1β), CCL9 (MIP-1γ), CCL10 (MIP-1α), CCL11 (MIP-1β), CCL12 (MIP-1γ), CCL13 (MIP-1α), CCL14 (MIP-1β), CCL15 (MIP-1γ), CCL16 (MIP-1α), CCL17 (MIP-1β), CCL18 (MIP-1γ), CCL19 (MIP-1α), CCL20 (MIP-1β), CCL21 (MIP-1γ), CCL22 (MIP-1α), CCL23 (MIP-1β), CCL24 (MIP-1γ), CCL25 (MIP-1α), CCL26 (MIP-1β), CCL27 (MIP-1γ), CCL28 (MIP-1α), CCL29 (MIP-1β), CCL30 (MIP-1γ)
CCR3	CCL3 (MIP-1γ), CCL4 (MIP-1δ), CCL5 (MIP-1β), CCL6 (MIP-1γ), CCL7 (MIP-1α), CCL8 (MIP-1β), CCL9 (MIP-1γ), CCL10 (MIP-1α), CCL11 (MIP-1β), CCL12 (MIP-1γ), CCL13 (MIP-1α), CCL14 (MIP-1β), CCL15 (MIP-1γ), CCL16 (MIP-1α), CCL17 (MIP-1β), CCL18 (MIP-1γ), CCL19 (MIP-1α), CCL20 (MIP-1β), CCL21 (MIP-1γ), CCL22 (MIP-1α), CCL23 (MIP-1β), CCL24 (MIP-1γ), CCL25 (MIP-1α), CCL26 (MIP-1β), CCL27 (MIP-1γ), CCL28 (MIP-1α), CCL29 (MIP-1β), CCL30 (MIP-1γ)
CCR4	CCL1 (MIP-1α), CCL2 (MIP-1β), CCL3 (MIP-1γ), CCL4 (MIP-1δ), CCL5 (MIP-1β), CCL6 (MIP-1γ), CCL7 (MIP-1α), CCL8 (MIP-1β), CCL9 (MIP-1γ), CCL10 (MIP-1α), CCL11 (MIP-1β), CCL12 (MIP-1γ), CCL13 (MIP-1α), CCL14 (MIP-1β), CCL15 (MIP-1γ), CCL16 (MIP-1α), CCL17 (MIP-1β), CCL18 (MIP-1γ), CCL19 (MIP-1α), CCL20 (MIP-1β), CCL21 (MIP-1γ), CCL22 (MIP-1α), CCL23 (MIP-1β), CCL24 (MIP-1γ), CCL25 (MIP-1α), CCL26 (MIP-1β), CCL27 (MIP-1γ), CCL28 (MIP-1α), CCL29 (MIP-1β), CCL30 (MIP-1γ)
CCR5	CCL3 (MIP-1γ), CCL4 (MIP-1δ), CCL5 (MIP-1β), CCL6 (MIP-1γ), CCL7 (MIP-1α), CCL8 (MIP-1β), CCL9 (MIP-1γ), CCL10 (MIP-1α), CCL11 (MIP-1β), CCL12 (MIP-1γ), CCL13 (MIP-1α), CCL14 (MIP-1β), CCL15 (MIP-1γ), CCL16 (MIP-1α), CCL17 (MIP-1β), CCL18 (MIP-1γ), CCL19 (MIP-1α), CCL20 (MIP-1β), CCL21 (MIP-1γ), CCL22 (MIP-1α), CCL23 (MIP-1β), CCL24 (MIP-1γ), CCL25 (MIP-1α), CCL26 (MIP-1β), CCL27 (MIP-1γ), CCL28 (MIP-1α), CCL29 (MIP-1β), CCL30 (MIP-1γ)
CCR6	CCL1 (MIP-1α), CCL2 (MIP-1β), CCL3 (MIP-1γ), CCL4 (MIP-1δ), CCL5 (MIP-1β), CCL6 (MIP-1γ), CCL7 (MIP-1α), CCL8 (MIP-1β), CCL9 (MIP-1γ), CCL10 (MIP-1α), CCL11 (MIP-1β), CCL12 (MIP-1γ), CCL13 (MIP-1α), CCL14 (MIP-1β), CCL15 (MIP-1γ), CCL16 (MIP-1α), CCL17 (MIP-1β), CCL18 (MIP-1γ), CCL19 (MIP-1α), CCL20 (MIP-1β), CCL21 (MIP-1γ), CCL22 (MIP-1α), CCL23 (MIP-1β), CCL24 (MIP-1γ), CCL25 (MIP-1α), CCL26 (MIP-1β), CCL27 (MIP-1γ), CCL28 (MIP-1α), CCL29 (MIP-1β), CCL30 (MIP-1γ)
CCR7	CCL1 (MIP-1α), CCL2 (MIP-1β), CCL3 (MIP-1γ), CCL4 (MIP-1δ), CCL5 (MIP-1β), CCL6 (MIP-1γ), CCL7 (MIP-1α), CCL8 (MIP-1β), CCL9 (MIP-1γ), CCL10 (MIP-1α), CCL11 (MIP-1β), CCL12 (MIP-1γ), CCL13 (MIP-1α), CCL14 (MIP-1β), CCL15 (MIP-1γ), CCL16 (MIP-1α), CCL17 (MIP-1β), CCL18 (MIP-1γ), CCL19 (MIP-1α), CCL20 (MIP-1β), CCL21 (MIP-1γ), CCL22 (MIP-1α), CCL23 (MIP-1β), CCL24 (MIP-1γ), CCL25 (MIP-1α), CCL26 (MIP-1β), CCL27 (MIP-1γ), CCL28 (MIP-1α), CCL29 (MIP-1β), CCL30 (MIP-1γ)
CCR8	CCL1 (MIP-1α), CCL2 (MIP-1β), CCL3 (MIP-1γ), CCL4 (MIP-1δ), CCL5 (MIP-1β), CCL6 (MIP-1γ), CCL7 (MIP-1α), CCL8 (MIP-1β), CCL9 (MIP-1γ), CCL10 (MIP-1α), CCL11 (MIP-1β), CCL12 (MIP-1γ), CCL13 (MIP-1α), CCL14 (MIP-1β), CCL15 (MIP-1γ), CCL16 (MIP-1α), CCL17 (MIP-1β), CCL18 (MIP-1γ), CCL19 (MIP-1α), CCL20 (MIP-1β), CCL21 (MIP-1γ), CCL22 (MIP-1α), CCL23 (MIP-1β), CCL24 (MIP-1γ), CCL25 (MIP-1α), CCL26 (MIP-1β), CCL27 (MIP-1γ), CCL28 (MIP-1α), CCL29 (MIP-1β), CCL30 (MIP-1γ)
CCR9	CCL1 (MIP-1α), CCL2 (MIP-1β), CCL3 (MIP-1γ), CCL4 (MIP-1δ), CCL5 (MIP-1β), CCL6 (MIP-1γ), CCL7 (MIP-1α), CCL8 (MIP-1β), CCL9 (MIP-1γ), CCL10 (MIP-1α), CCL11 (MIP-1β), CCL12 (MIP-1γ), CCL13 (MIP-1α), CCL14 (MIP-1β), CCL15 (MIP-1γ), CCL16 (MIP-1α), CCL17 (MIP-1β), CCL18 (MIP-1γ), CCL19 (MIP-1α), CCL20 (MIP-1β), CCL21 (MIP-1γ), CCL22 (MIP-1α), CCL23 (MIP-1β), CCL24 (MIP-1γ), CCL25 (MIP-1α), CCL26 (MIP-1β), CCL27 (MIP-1γ), CCL28 (MIP-1α), CCL29 (MIP-1β), CCL30 (MIP-1γ)
CXCR1	CXCL1 (fractalkine), CXCL2 (lymphotactin), CXCL3 (MIP-1α), CXCL4 (MIP-1β), CXCL5 (MIP-1γ), CXCL6 (MIP-1δ), CXCL7 (MIP-1ε), CXCL8 (MIP-1ζ), CXCL9 (MIP-1η), CXCL10 (MIP-1θ), CXCL11 (MIP-1ι), CXCL12 (MIP-1κ), CXCL13 (MIP-1λ), CXCL14 (MIP-1μ), CXCL15 (MIP-1ν), CXCL16 (MIP-1ξ), CXCL17 (MIP-1ο), CXCL18 (MIP-1π), CXCL19 (MIP-1ρ), CXCL20 (MIP-1σ), CXCL21 (MIP-1τ), CXCL22 (MIP-1υ), CXCL23 (MIP-1φ), CXCL24 (MIP-1χ), CXCL25 (MIP-1ψ), CXCL26 (MIP-1ω), CXCL27 (MIP-1x), CXCL28 (MIP-1z), CXCL29 (MIP-1aa), CXCL30 (MIP-1ab)
CXCR2	CXCL1 (fractalkine), CXCL2 (lymphotactin), CXCL3 (MIP-1α), CXCL4 (MIP-1β), CXCL5 (MIP-1γ), CXCL6 (MIP-1δ), CXCL7 (MIP-1ε), CXCL8 (MIP-1ζ), CXCL9 (MIP-1η), CXCL10 (MIP-1θ), CXCL11 (MIP-1ι), CXCL12 (MIP-1κ), CXCL13 (MIP-1λ), CXCL14 (MIP-1μ), CXCL15 (MIP-1ν), CXCL16 (MIP-1ξ), CXCL17 (MIP-1ο), CXCL18 (MIP-1π), CXCL19 (MIP-1ρ), CXCL20 (MIP-1σ), CXCL21 (MIP-1τ), CXCL22 (MIP-1υ), CXCL23 (MIP-1φ), CXCL24 (MIP-1χ), CXCL25 (MIP-1ψ), CXCL26 (MIP-1ω), CXCL27 (MIP-1x), CXCL28 (MIP-1z), CXCL29 (MIP-1aa), CXCL30 (MIP-1ab)
CXCR3	CXCL1 (fractalkine), CXCL2 (lymphotactin), CXCL3 (MIP-1α), CXCL4 (MIP-1β), CXCL5 (MIP-1γ), CXCL6 (MIP-1δ), CXCL7 (MIP-1ε), CXCL8 (MIP-1ζ), CXCL9 (MIP-1η), CXCL10 (MIP-1θ), CXCL11 (MIP-1ι), CXCL12 (MIP-1κ), CXCL13 (MIP-1λ), CXCL14 (MIP-1μ), CXCL15 (MIP-1ν), CXCL16 (MIP-1ξ), CXCL17 (MIP-1ο), CXCL18 (MIP-1π), CXCL19 (MIP-1ρ), CXCL20 (MIP-1σ), CXCL21 (MIP-1τ), CXCL22 (MIP-1υ), CXCL23 (MIP-1φ), CXCL24 (MIP-1χ), CXCL25 (MIP-1ψ), CXCL26 (MIP-1ω), CXCL27 (MIP-1x), CXCL28 (MIP-1z), CXCL29 (MIP-1aa), CXCL30 (MIP-1ab)
CXCR4	CXCL1 (fractalkine), CXCL2 (lymphotactin), CXCL3 (MIP-1α), CXCL4 (MIP-1β), CXCL5 (MIP-1γ), CXCL6 (MIP-1δ), CXCL7 (MIP-1ε), CXCL8 (MIP-1ζ), CXCL9 (MIP-1η), CXCL10 (MIP-1θ), CXCL11 (MIP-1ι), CXCL12 (MIP-1κ), CXCL13 (MIP-1λ), CXCL14 (MIP-1μ), CXCL15 (MIP-1ν), CXCL16 (MIP-1ξ), CXCL17 (MIP-1ο), CXCL18 (MIP-1π), CXCL19 (MIP-1ρ), CXCL20 (MIP-1σ), CXCL21 (MIP-1τ), CXCL22 (MIP-1υ), CXCL23 (MIP-1φ), CXCL24 (MIP-1χ), CXCL25 (MIP-1ψ), CXCL26 (MIP-1ω), CXCL27 (MIP-1x), CXCL28 (MIP-1z), CXCL29 (MIP-1aa), CXCL30 (MIP-1ab)
CXCR5	CXCL1 (fractalkine), CXCL2 (lymphotactin), CXCL3 (MIP-1α), CXCL4 (MIP-1β), CXCL5 (MIP-1γ), CXCL6 (MIP-1δ), CXCL7 (MIP-1ε), CXCL8 (MIP-1ζ), CXCL9 (MIP-1η), CXCL10 (MIP-1θ), CXCL11 (MIP-1ι), CXCL12 (MIP-1κ), CXCL13 (MIP-1λ), CXCL14 (MIP-1μ), CXCL15 (MIP-1ν), CXCL16 (MIP-1ξ), CXCL17 (MIP-1ο), CXCL18 (MIP-1π), CXCL19 (MIP-1ρ), CXCL20 (MIP-1σ), CXCL21 (MIP-1τ), CXCL22 (MIP-1υ), CXCL23 (MIP-1φ), CXCL24 (MIP-1χ), CXCL25 (MIP-1ψ), CXCL26 (MIP-1ω), CXCL27 (MIP-1x), CXCL28 (MIP-1z), CXCL29 (MIP-1aa), CXCL30 (MIP-1ab)
CXCR7	CXCL1 (fractalkine), CXCL2 (lymphotactin), CXCL3 (MIP-1α), CXCL4 (MIP-1β), CXCL5 (MIP-1γ), CXCL6 (MIP-1δ), CXCL7 (MIP-1ε), CXCL8 (MIP-1ζ), CXCL9 (MIP-1η), CXCL10 (MIP-1θ), CXCL11 (MIP-1ι), CXCL12 (MIP-1κ), CXCL13 (MIP-1λ), CXCL14 (MIP-1μ), CXCL15 (MIP-1ν), CXCL16 (MIP-1ξ), CXCL17 (MIP-1ο), CXCL18 (MIP-1π), CXCL19 (MIP-1ρ), CXCL20 (MIP-1σ), CXCL21 (MIP-1τ), CXCL22 (MIP-1υ), CXCL23 (MIP-1φ), CXCL24 (MIP-1χ), CXCL25 (MIP-1ψ), CXCL26 (MIP-1ω), CXCL27 (MIP-1x), CXCL28 (MIP-1z), CXCL29 (MIP-1aa), CXCL30 (MIP-1ab)
BLT1	CXCL1 (fractalkine), CXCL2 (lymphotactin), CXCL3 (MIP-1α), CXCL4 (MIP-1β), CXCL5 (MIP-1γ), CXCL6 (MIP-1δ), CXCL7 (MIP-1ε), CXCL8 (MIP-1ζ), CXCL9 (MIP-1η), CXCL10 (MIP-1θ), CXCL11 (MIP-1ι), CXCL12 (MIP-1κ), CXCL13 (MIP-1λ), CXCL14 (MIP-1μ), CXCL15 (MIP-1ν), CXCL16 (MIP-1ξ), CXCL17 (MIP-1ο), CXCL18 (MIP-1π), CXCL19 (MIP-1ρ), CXCL20 (MIP-1σ), CXCL21 (MIP-1τ), CXCL22 (MIP-1υ), CXCL23 (MIP-1φ), CXCL24 (MIP-1χ), CXCL25 (MIP-1ψ), CXCL26 (MIP-1ω), CXCL27 (MIP-1x), CXCL28 (MIP-1z), CXCL29 (MIP-1aa), CXCL30 (MIP-1ab)

Methodology

total RNA in a 50 µl reaction
 6 samples of 2.00 µl of each type of cell – 3LL, p-3LL, tumor and p-tumor, underwent real time PCR in the presence of 2.00 µl of primers for every one of the chemokine receptors
 6.00 µl of water and 10.00 µl of SyBr green mix was added to the 96 well plate
 Direct detection of PCR products was monitored by measuring the increase in fluorescence caused by the binding of SYBR green 1 dye to double strand DNA
 The parameter Ct (threshold cycle) was defined as the fraction cycle number at which the fluorescence passed the threshold
 The relative gene expression is compared with control (untreated/housekeeping gene) using 2^{-ΔΔCt} method by normalizing with GAPDH gene expression in all the experiments

Fig. 4: Differential expression of each chemokine receptor at transcript levels in 3LL tumors compared to p-3LL tumors

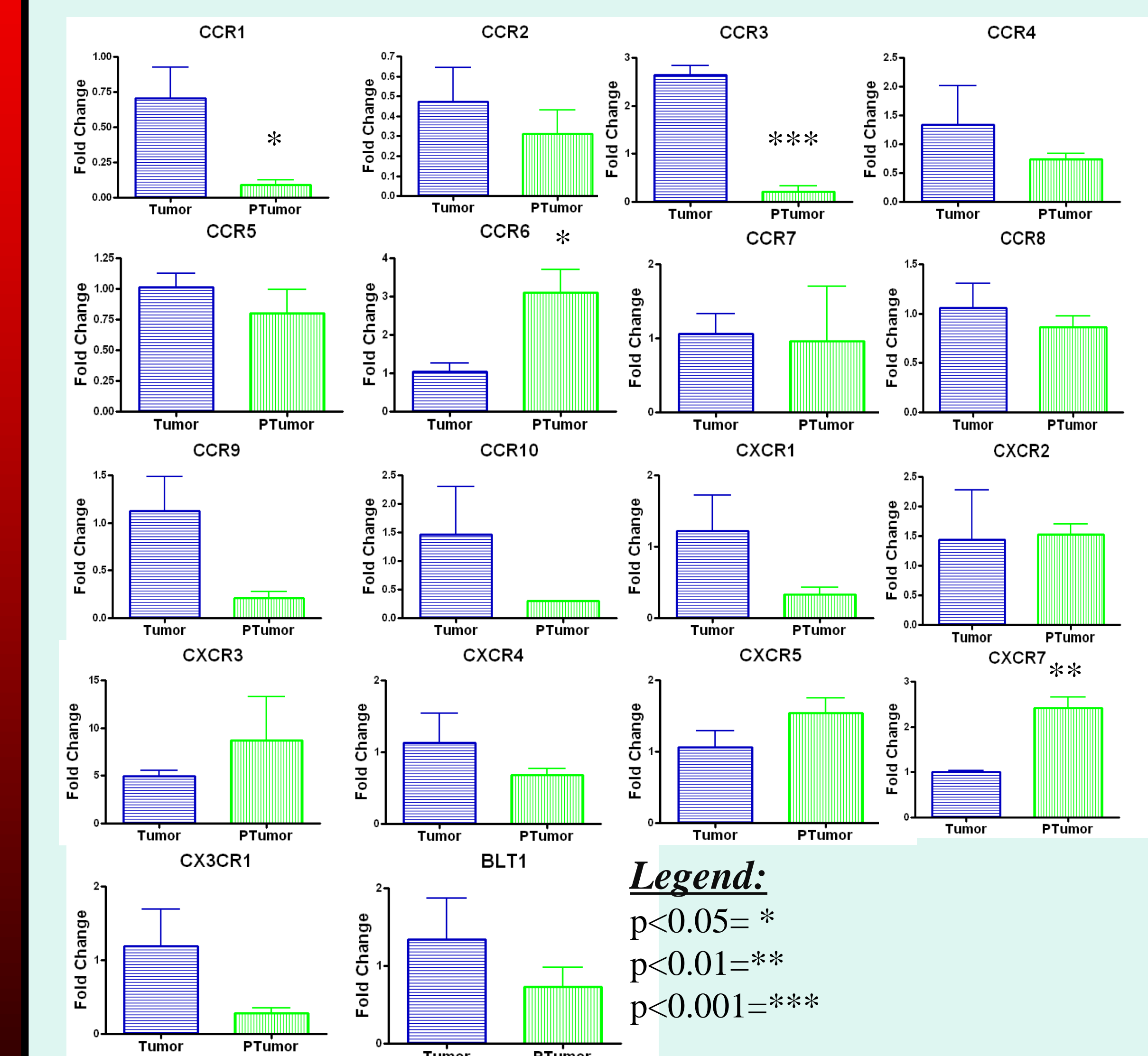
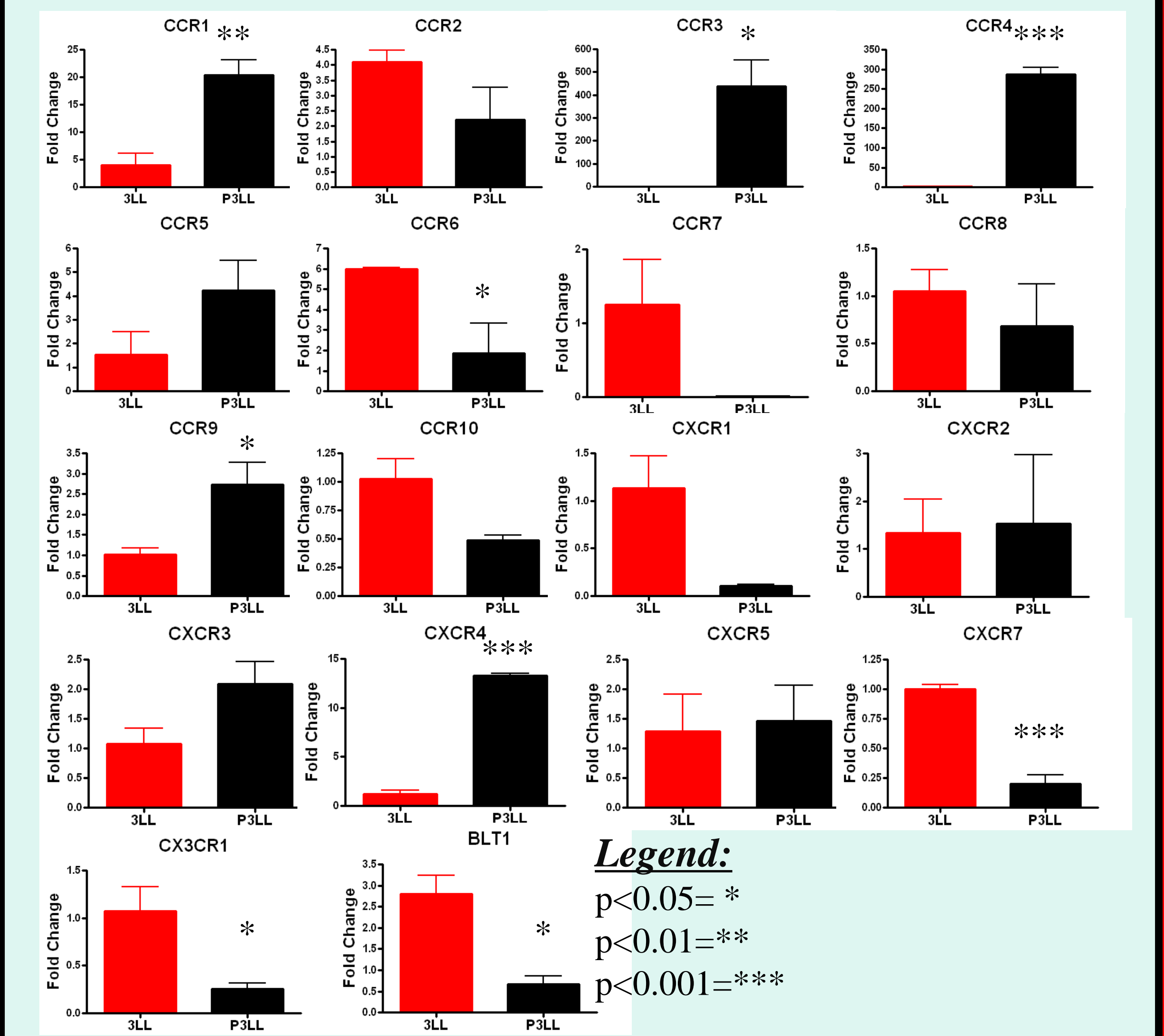


Fig. 5: Differential expression of each chemokine receptors at transcript levels in 3LL cells compared to p-3LL cells



Summary and Conclusion

Successful establishment of a poorly and highly metastatic spontaneous animal model for lung cancer (Fig. 1).

3LL cells show minimal metastasis, while p-3LL cells show robust metastasis in subcutaneous model of spontaneous metastasis (Fig. 2).

Chemokine receptors CCR1 and CCR3 were found to be down-regulated in the passage tumors (Fig. 5).

Chemokine receptors CCR6 and CXCR7 were found to be up-regulated in the passage tumors. (Fig. 5).

CCR6, CXCR1, CXCR7, CX3CR1, and BLT1 were found to be down-regulated in p-3LL cells compared to 3LL cells (Fig. 6).

CCR1, CCR3, CCR4, CCR9, and CXCR4 were found to be up-regulated in the highly metastatic p-3LL cells compared to the 3LL cells (Fig. 6).

In conclusion, the study defines a distinct pattern of chemokine receptors which could potentially play pro or anti-metastatic role in our model of 3LL cancer cell and tumor metastasis. The significant up-regulation of the chemokine receptors in the p-3LL cells but not the p-tumors may indicate that those receptors on the host cells may play a role in metastasis. Further studies are needed to confirm the differential expression of various receptors in 3-LL and P-3LL cells. The functional significance of individual chemokine receptors will have to be confirmed by independent siRNA and inhibitor experiments.

Acknowledgements: Supported by grant R25-CA134283 from the National Cancer Institute

Stable Isotope Resolved Metabolomics Reveals Functional Biochemistry in Primary Non Small Cell Lung Cancer Cell Line

Connor J. Kinslow,¹ Teresa W.M. Fan, Ph.D.,² Jin Lian Tan, M.S.,¹ Pawel K Lorkiewicz, Ph.D.,² Ramya Balasubramaniam, M.S.,² Andrew N. Lane, Ph.D.¹
James Graham Brown Cancer Center¹ and Department of Biochemistry²
University of Louisville School of Medicine

1. Introduction

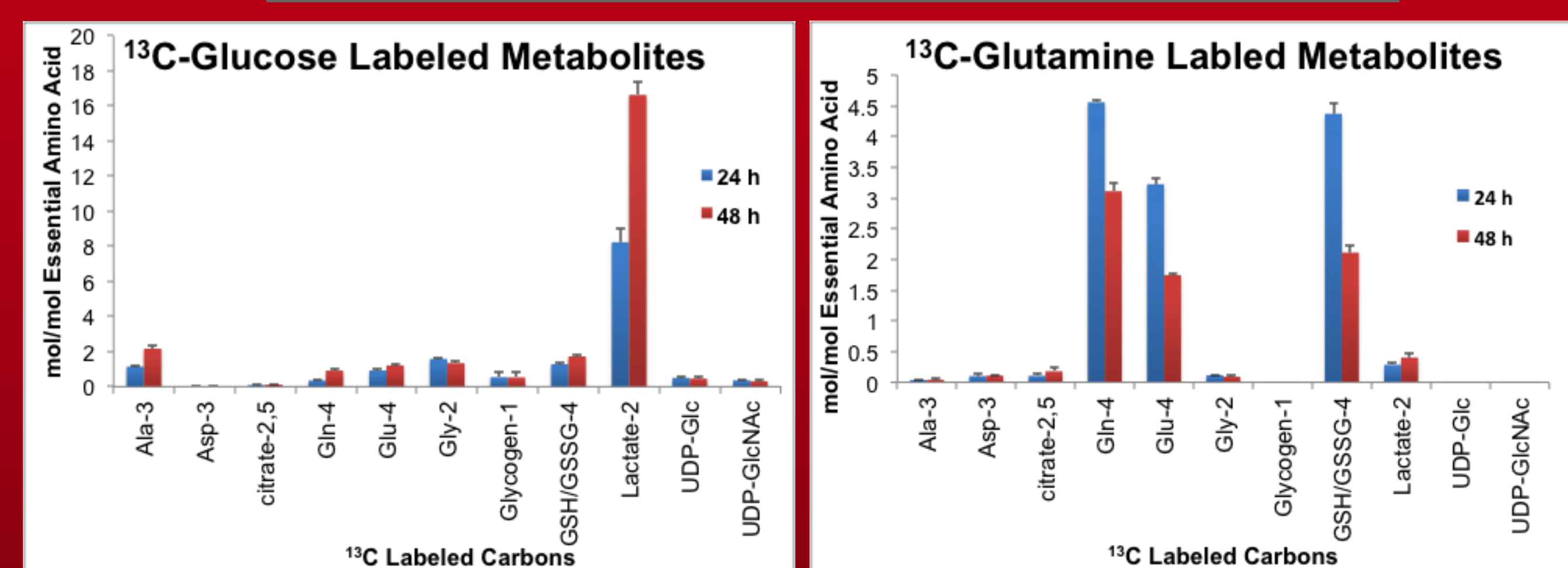
Lung cancer is the second leading cause of death nationwide. 5-year survival rate for localized cancer (52.5%) is much higher than for advanced stages (3.5%).¹ However, only 15% of patients are diagnosed at this early stage.¹ Development of early stage biomarkers will drastically decrease death rates. Stable isotope-resolved metabolomics (SIRM) provides a functional readout of cellular activity and is therefore a useful tool in biomarker discovery and fundamental cancer biology. We have established a primary lung squamous cell carcinoma line (PSLC1) in collaboration with Dr. Jun Yan, and studied it in situ and in mouse xenografts using SIRM. Here we report the metabolic activities of the cell line in culture using two different tracers to evaluate central metabolism.

2. Methods

PSLC1 cells were grown in either [U-¹³C]-glucose or [U-¹³C,¹⁵N]-glutamine labeled medium. Cell extracts and medium were prepared and analyzed by ¹H-NMR, HSQC, TOCSY, GC-MS, and FTICR-MS.²⁻⁴

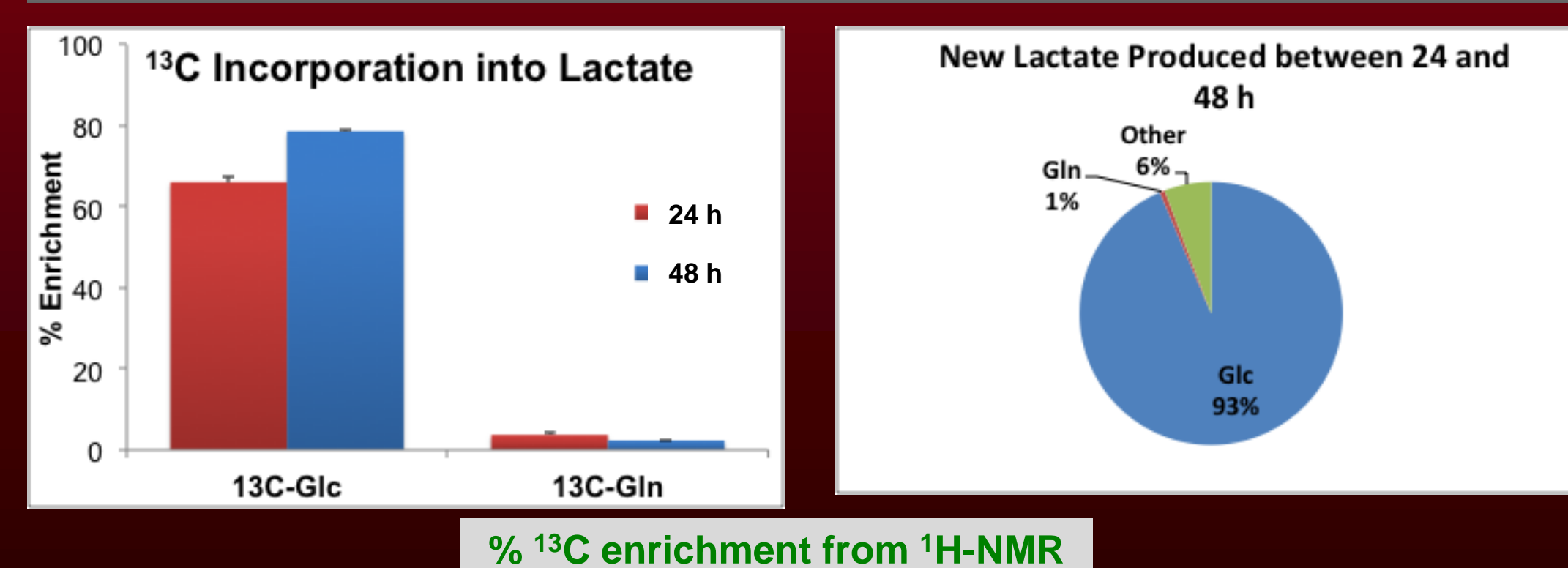
3. Results

4. Metabolic Profiles of PSLC1 cells



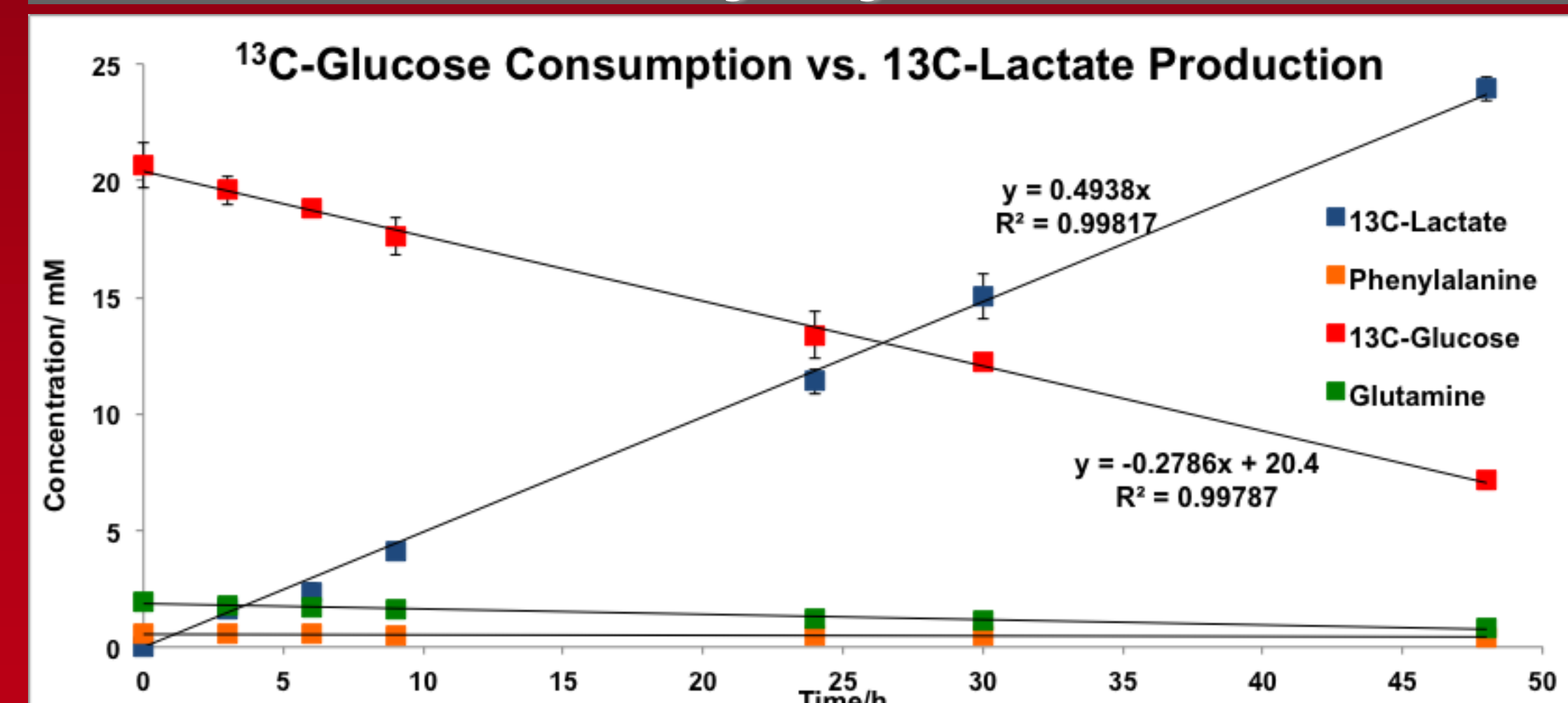
Cells were grown in the presence of either [U-¹³C]-glucose or [U-¹³C,¹⁵N]-Gln for 24 and 48 h prior to harvesting and extracting. The HSQC NMR selects protons directly attached to ¹³C, and can be quantified.

5. Lactate Derives from Glucose



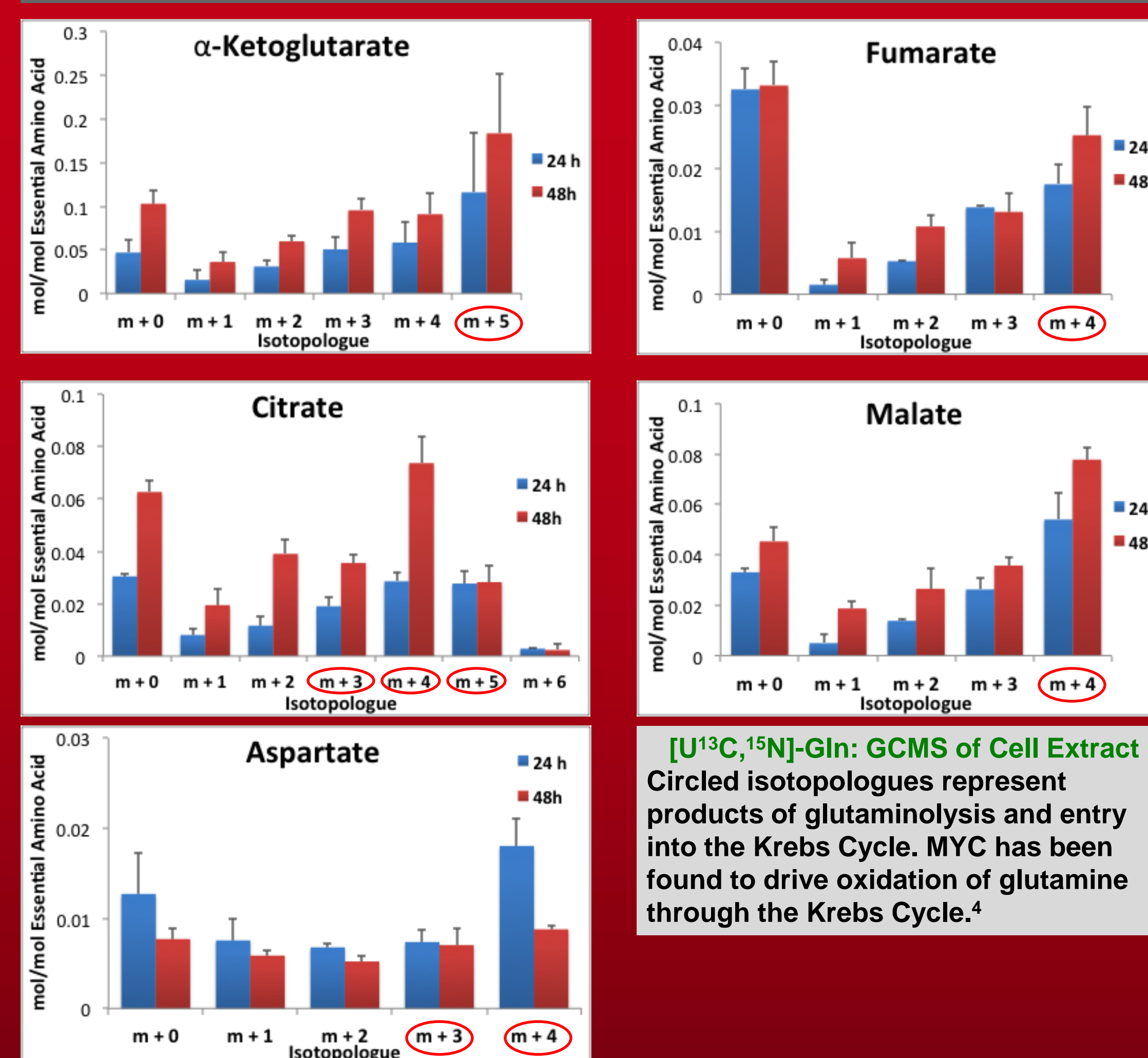
% ¹³C enrichment from ¹H-NMR

6. Glucose Consumption and Lactate Production Indicate That the Cells Are Highly Glycolytic



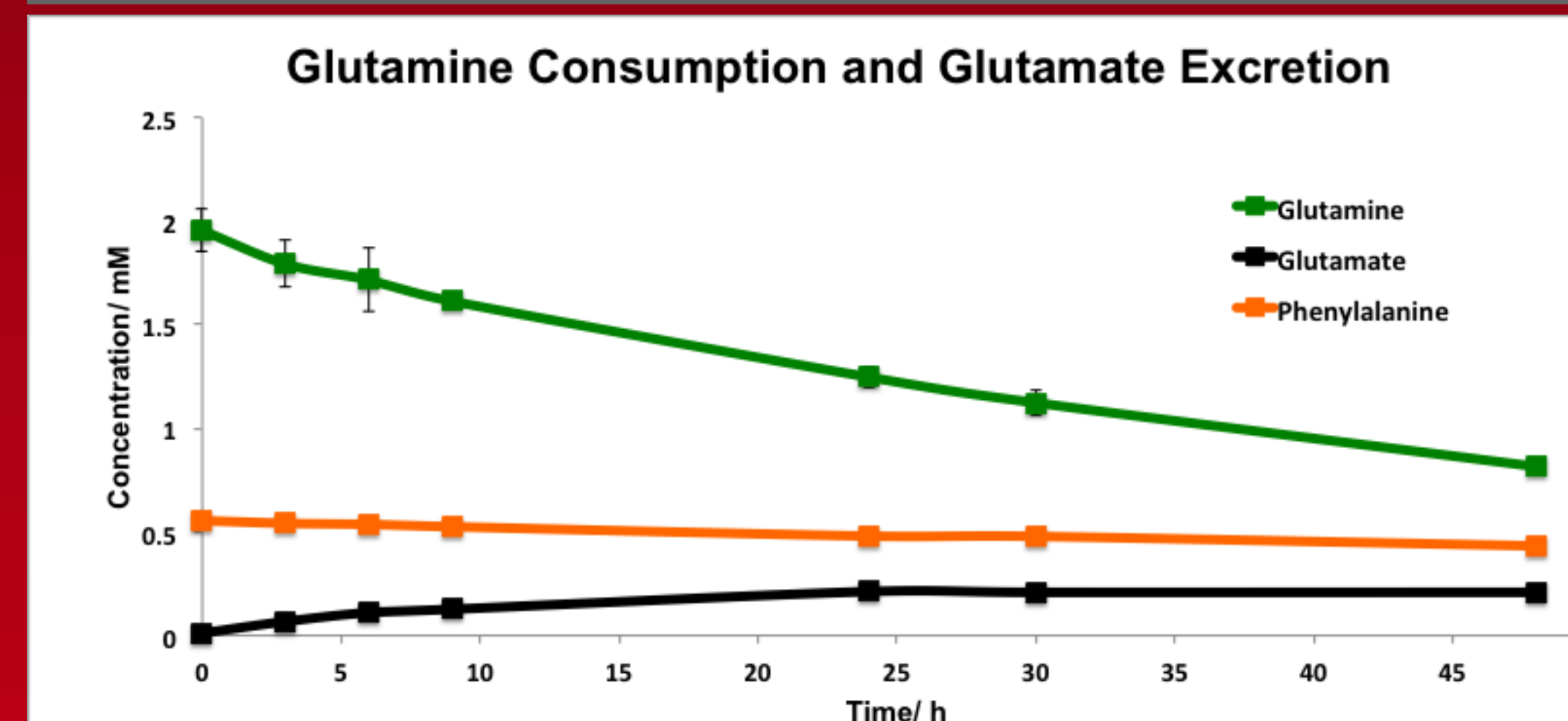
Glucose consumption and lactate production in the medium were determined using ¹H-NMR. 88.6 ± 2.9% of the glucose consumed was converted to excreted lactate. The rate of Gln consumption was <10% of the glucose consumption rate.

8. Glucose-Independent TCA Cycling from Glutamine



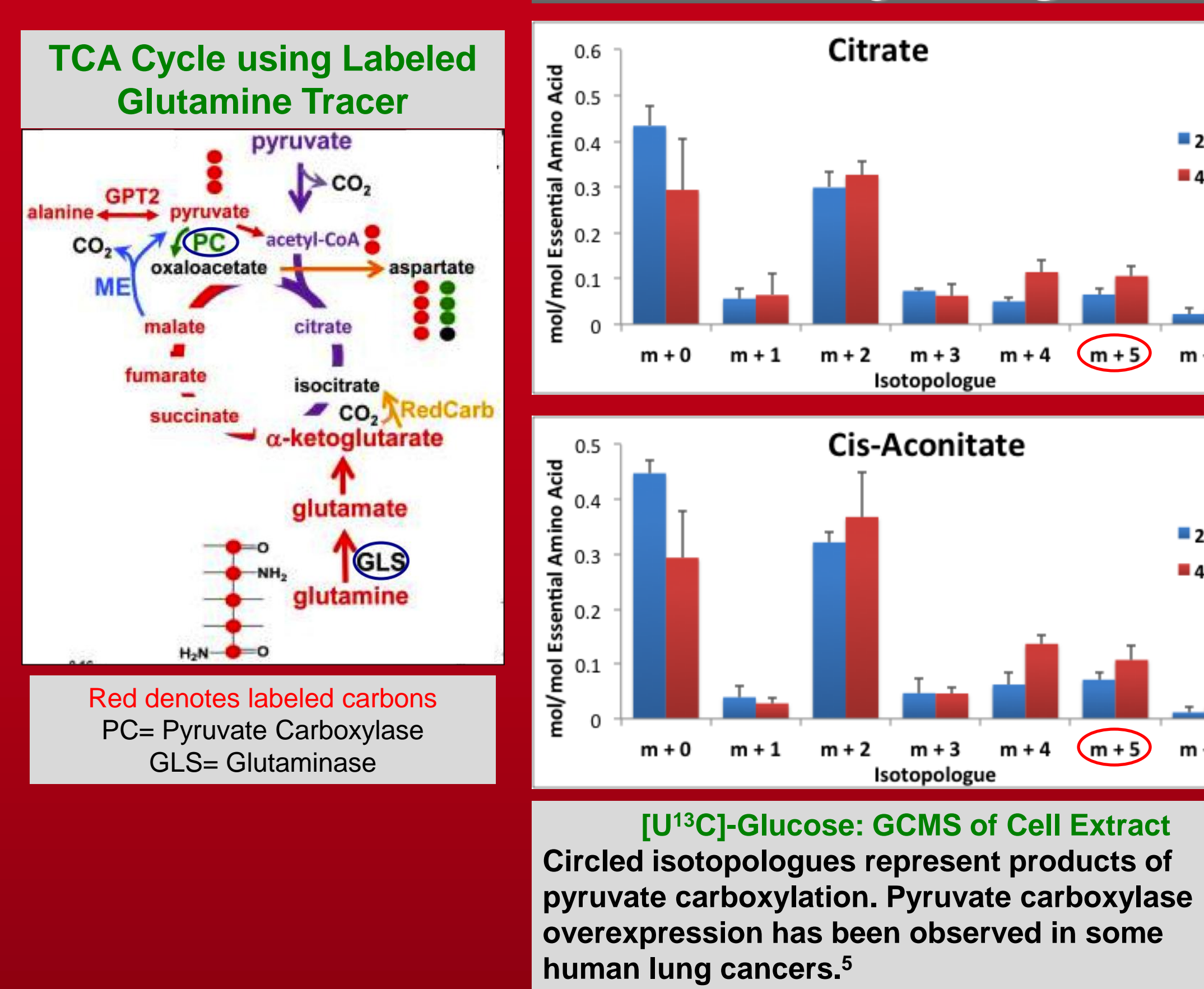
[U-¹³C,¹⁵N]-Gln: GCMS of Cell Extract Circled isotopologues represent products of glutaminolysis and entry into the Krebs Cycle. MYC has been found to drive oxidation of glutamine through the Krebs Cycle.⁴

7. Cells Consume Glutamine and Excrete Glutamate



Approximately 15% of the Gln consumed was converted to Glu and excreted, implying active glutaminolysis and a possible amino acid antiport activity.

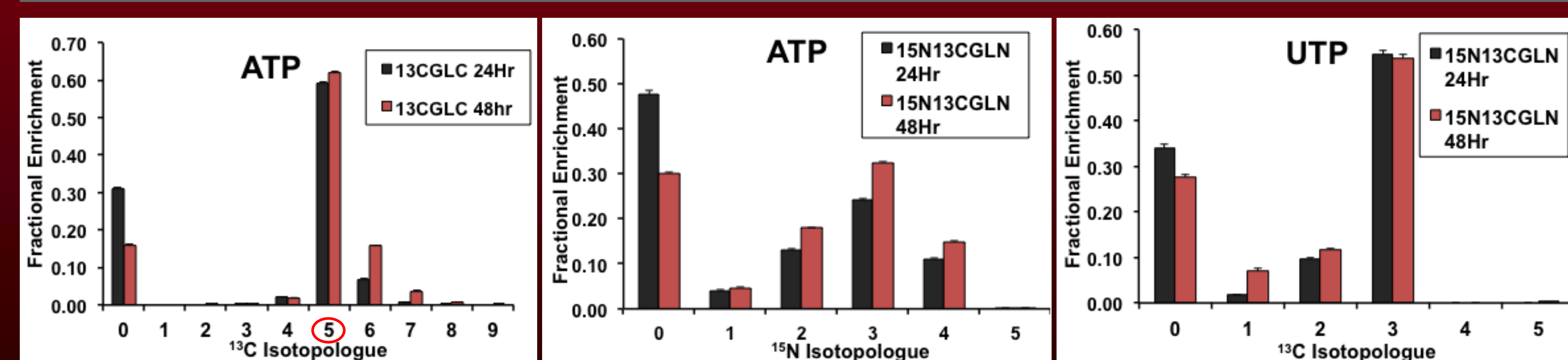
9. Pyruvate Carboxylase Activity is High



Red denotes labeled carbons
PC= Pyruvate Carboxylase
GLS= Glutaminase

[U-¹³C]-Glucose: GCMS of Cell Extract Circled isotopologues represent products of pyruvate carboxylation. Pyruvate carboxylase overexpression has been observed in some human lung cancers.⁵

10. Glucose and Glutamine in De Novo Nucleotide Biosynthesis



[U-¹³C]-glucose: ATP (m + 5) isotopologue indicates that the ribose subunit is derived from glucose.

[U-¹³C,¹⁵N]-Glutamine: Glutamine is a major nitrogen donor in purine biosynthesis.

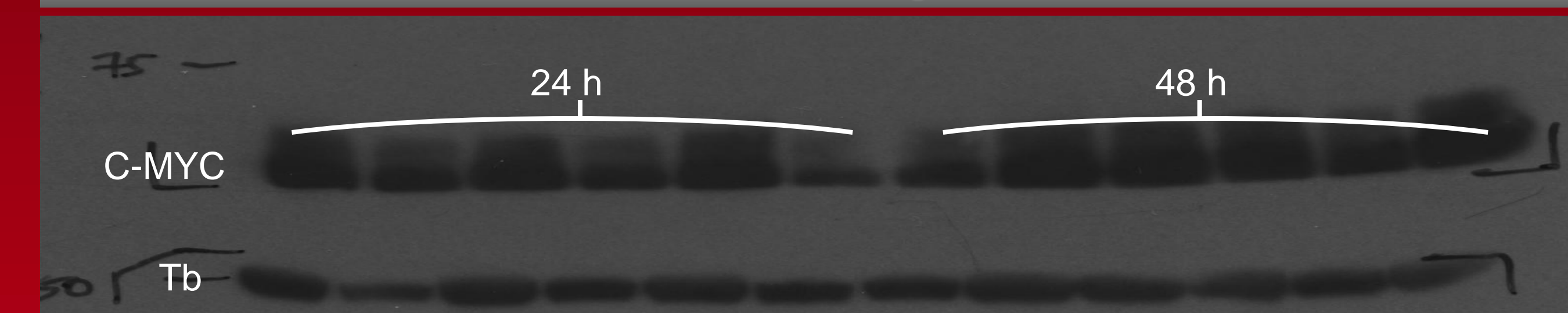
[U-¹³C,¹⁵N]-Glutamine: Glutamine is the dominant carbon source for pyrimidine biosynthesis.

11. Glutamine is the Major Precursor in Proline Biosynthesis

Isotopomer	24h:Glc	48h:Glc	24h:Gln	48h:Gln
Proline	>95	>95	<10	<10
¹² C ₂ - ¹³ C _{3,4}	<5	<5	>90	>90
¹³ C ₂ - ¹³ C _{3,4}	<5	<5	>90	>90

% ¹³C enrichment was determined from 2D TOCSY experiments: Pro is heavily enriched from Gln, and insignificantly from Glc. C-MYC has been found to up-regulate enzymes involved in proline biosynthesis.⁶

12. Pro-META Analysis Confirms C-MYC Overexpression



NSCLC are often MYC-driven. Western Blot using anti-C-MYC and anti-Tubulin shows high expression of MYC in these cells.

13. Discussion

- C-MYC overexpression was determined by Western Blot analysis combined with SIRM via Pro-META analysis⁷
- Cells exhibited linear glucose consumption that persisted even as consumption of other nutrients diminished
- Glutamine represents a major contributor for biosynthetic and bioenergetic cellular needs
- Glutaminase and enzymes involved in proline metabolism may be up-regulated by C-MYC overexpression^{4,6}
- SIRM indicates that pyruvate carboxylase may be up-regulated⁴⁻⁵

The ability of SIRM to generate hypotheses about protein expression demonstrates its potential use as a first line biomarker detection method. Comparison of cell culture data with upstream in situ and xenograft data will allow us to assess model validity and the effects of tumor microenvironment, which will help us interpret human in situ data more reliably.

14. References

- U.S. National Institutes of Health. National Cancer Institute: SEER Cancer Statistics Review, 1973-2008
- Lane, A.N. & Fan, T. W.-M. (2007) "Determination of positional isotopomers in metabolites". *Metabolomics* 3, 79-86
- Lane, A.N., Fan, T.-W.M. & Higashi, R.M. (2008) "Isotopomer-based metabolomic analysis by NMR and mass spectrometry". *Methods in Cell Biology, Vol 84. Biophysical Tools for Biologists, Volume 1*, edited by Drs. John J. Correia and H. William Detrich. Elsevier Science & Technology Books Ch. 18, pp 541-588
- Le, A., Lane, A. N., Hamaker, M., Bose, S., Gouw, A., Barbi, J., Tsukamoto, T., Rojas, C. J., Slusher, B. S., Zhang, H., Zimmerman, L. J., Liebler, D. C., Slebos, R. J., Lorkiewicz, P. K., Higashi, R. M., Fan, T. W., and Dang, C. V. (2012) "Glucose-independent glutamine metabolism via TCA cycling for proliferation and survival in B cells". *Cell Metabolism* 15, 110-121.
- Fan, T. W., Lane, A. N., Higashi, R. M., Farag, M. A., Gao, H., Bousamra, M., and Miller, D. M. (2009) "Altered regulation of metabolic pathways in human lung cancer discerned by ¹³C stable isotope-resolved metabolomics (SIRM)". *Mol Cancer* 8, 1476-4598.
- Liu, W., Le, A., Hancock, C., Lane, A. N., Dang, C. V., Fan, T. W., and Phang, J. M. (2012) "Reprogramming of proline and glutamine metabolism contributes to the proliferative and metabolic responses regulated by oncogenic transcription factor c-MYC". *Proceedings of the National Academy of Sciences of the United States of America* 109, 8983-8988.
- Fan, T.W.-M., et al. (2005) "Metabolomics-edited transcriptomics analysis of Se anticancer action in human lung cancer cells". *Metabolomics* 1, 325-339

15. Acknowledgements

This work was supported by grants R25-CA134283-01A2 (Hein), P01CA163223-01A1 (Lane), P20GM103482 (Miller), NSF EPSCoR EPS-0447479 (Fan) and EPS-0132295 (Wittebort), and the National Cancer Institute R25 Cancer Education Program.

Developing SOX9 Inhibitors

Danial A. Malik¹, John O. Trent^{2,3}, Mohammad T. Malik^{2,3}, and Paula J Bates^{2,3}

University of Louisville, College of Arts & Sciences¹ and School of Medicine, Departments of Medicine² and

Biochemistry & Molecular Biology³

University of Louisville, Louisville. Kentucky.

Abstract:

Cancer is the second leading cause of deaths in the United States. Current treatments lead to long-term survival in about two-thirds of people with cancer, but with increasing incidence rates for some cancers and an aging population the need for improved therapies remains. To maximize effectiveness while minimizing side effects, it is preferable to target molecules that are both specifically overexpressed in cancer cells and critical for cancer cell survival. The SOX9 transcription factor performs important functions during embryogenesis, but is rarely expressed in adult cells. Recent findings indicate that SOX9 expression is reactivated in many cancers and SOX9 has emerged as a master regulator of cancer stem cells (a subset of aggressive cancer cells that mediate recurrence and metastasis). Thus, small molecule inhibitors of SOX9 are exciting prospects as anticancer drugs. The purpose of this project was to evaluate compounds that had been identified as candidate SOX9 inhibitors by a virtual screening approach. Following computational screening of 2.1 million compounds for their binding to defined sites within a homology model of SOX9, a total of 182 compounds were selected for analysis. Their effects on the proliferation of SOX9-expressing cancer cells were determined using a colorimetric assay. Initial cell-based screening identified 10 compounds for further analysis and additional experiments were performed to assess cancer-selectivity and chemical stability. This allowed us to identify two compounds that show the most promising activity and selectivity for malignant vs. non-malignant cells. Supported in part by grant R25-CA-134283.

Introduction:

❖ Current treatments options for cancer include chemotherapies, targeted therapies, radiation, and/or surgery. These treatments have contributed to a 68% survival rate in all cancers among adults, but with increase in incident rates and population there is a need for new targeted therapies¹.

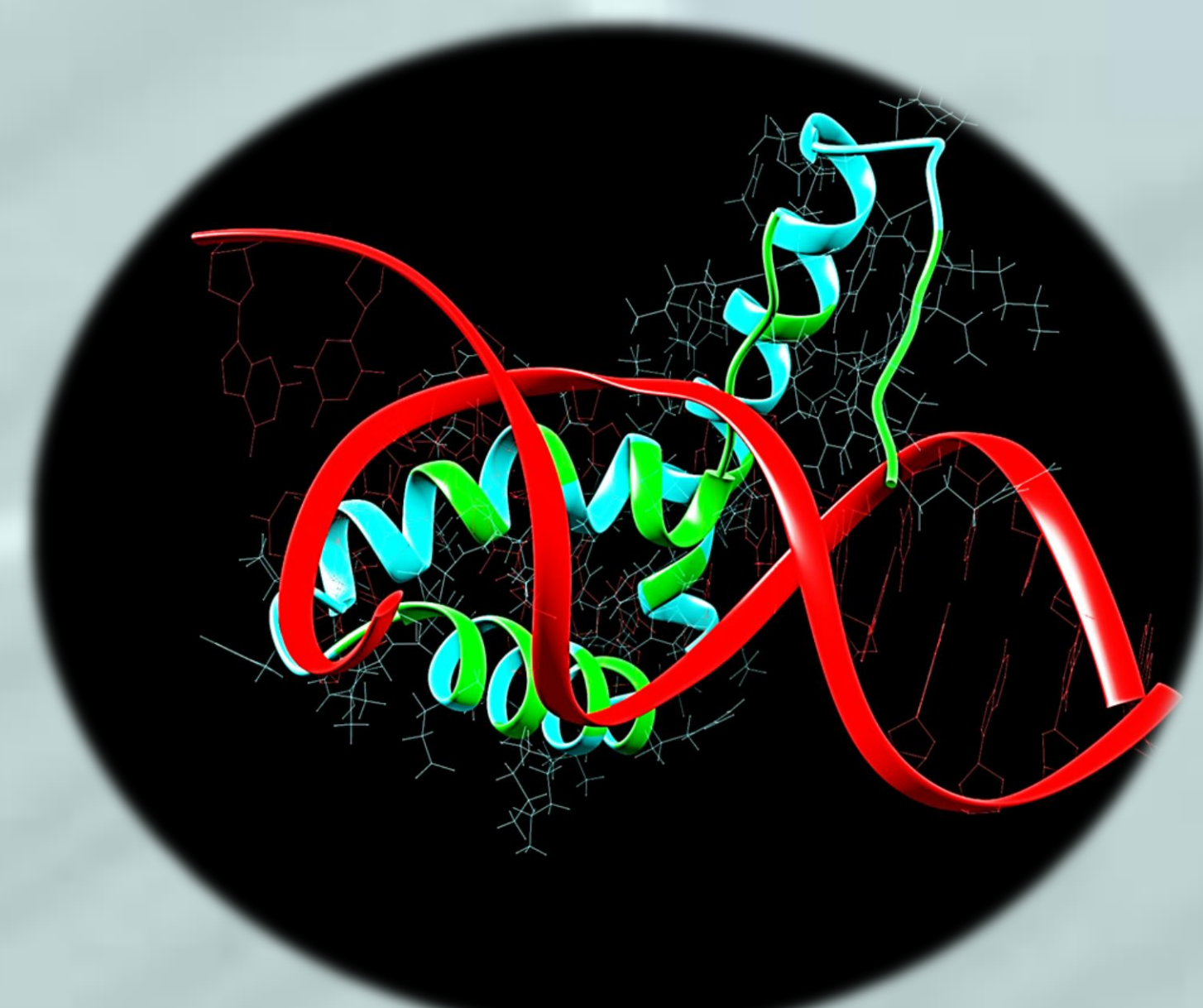
❖ To maximize effectiveness and specificity, new drug development is highly concentrated on targets whose expression is linked to cancer progression.

❖ SOX9 is a transcription factor characterized by the high mobility group (HMG) DNA-binding domain and is a member of the SRY (sex determining region Y) gene superfamily.

❖ SOX9 has various critical functions during embryogenesis such as sex determination, cartilage, skeleton and organ development, but is not expressed in most adult cells².

❖ Recently SOX9 has been implicated as a proto-oncogene in many cancers with roles in tumor development through cell cycle regulatory mechanisms³.

❖ Thus finding key inhibitors to SOX9 transcription factor would reduce the tumor progression which can serve as a potential drug therapy in the future.



Using the high mobility group (HMG) DNA-binding domain of SOX17, a homology model of SOX9 was created, shown in the picture above. The DNA binding region of the SOX9 model was then targeted in two sections due to the extended DNA contact area, generating two protomols, or complementary theoretical ligands. These protomols with the SOX9 homology model were used as configurations to screen for any matching compounds within the 2012 Morplex Library.

Figure 1: Molecular Model of SOX9 bound to DNA

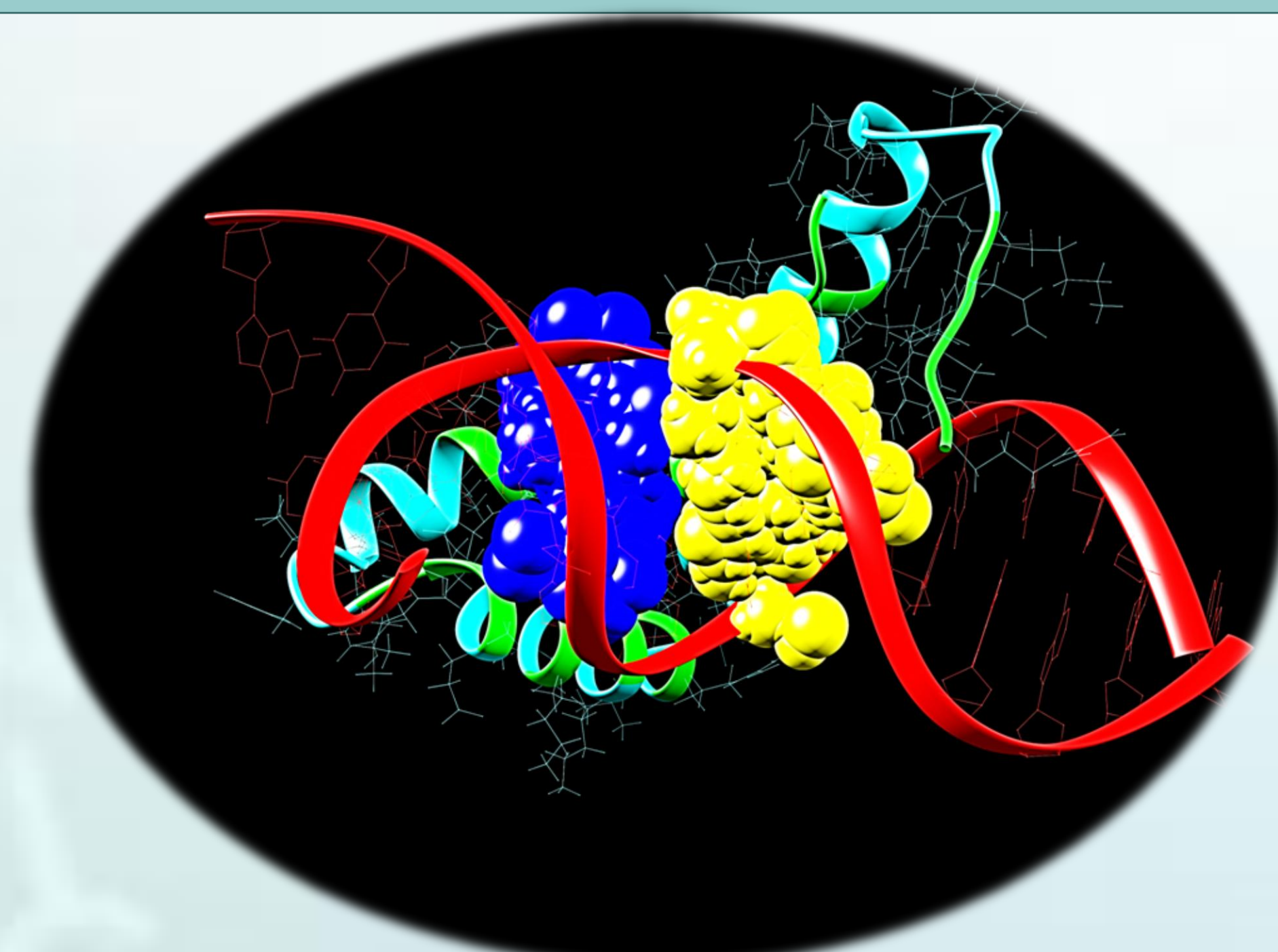


Figure 1: A SOX9 homology model constructed from the HMG DNA-binding domain of SOX17 (72% identity and 85% positives with SOX9) using Prime (Schrodinger)⁴. The two "protomols", generated using proto_thresh 0.18 and proto_bloat 0, shown in yellow and blue, and the SOX9 model were then used with SurflexDock (v 2.601)⁵ to screen the 2012 Morplex Library containing 2,100,000 compounds. The top 96 compounds from each virtual screen for both protomols were purchased for further screen in vitro

Figure 4: Malignant vs. Non-Malignant Comparison of Compound A9

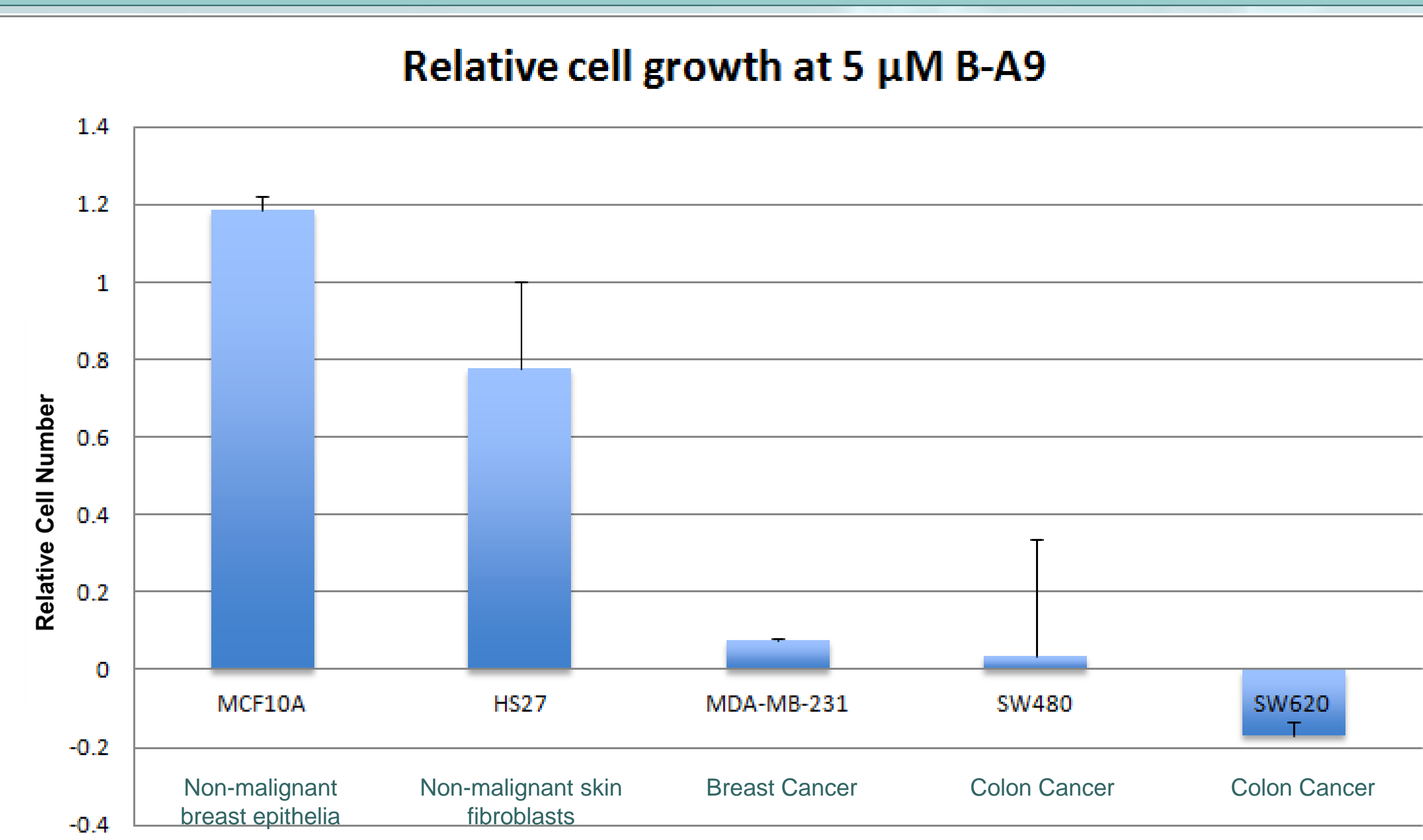


Figure 4: MTT Assay: Compound B-A9 (5uM) shows specific antiproliferative activity against malignant cells, MDA-MB231 (breast cancer), SW-480, & SW-620 (colon cancer), whereas there was little or no effect on non-malignant cells, Hs27 (skin fibroblast) and MCF10A (breast epithelial).

Acknowledgments:

Research supported by grant from R25-CA-134283 from The National Cancer Institute (NCI) Cancer Education Program, the University of Louisville School of Medicine, & the James Graham Brown Cancer Center.

Results:

Figure 2: Screen of Selected Compounds in Cancer Cells

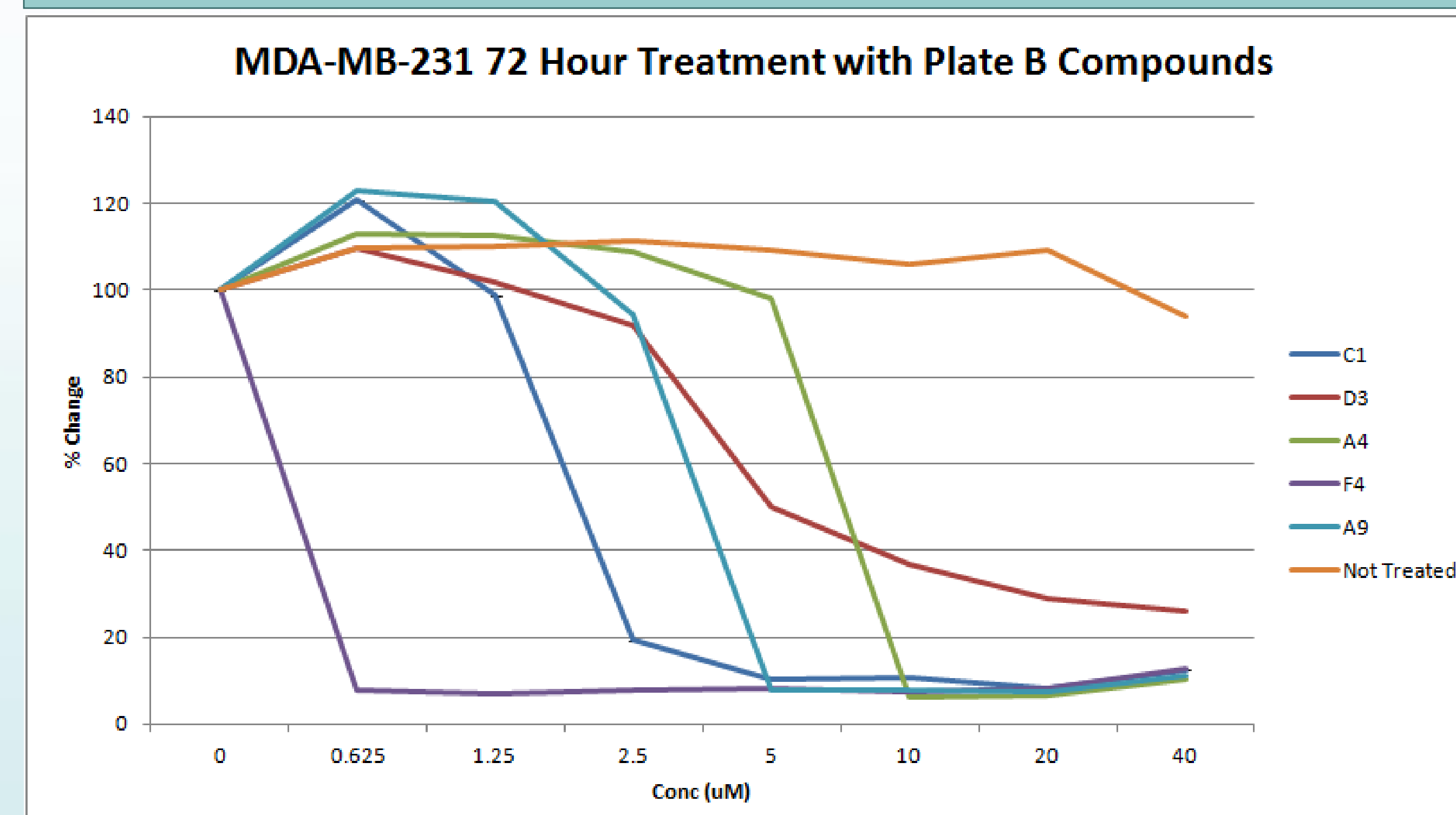


Figure 2-3: MTT Assay: MDA-MB-231 breast adenocarcinoma cells were first treated with 182 compounds to screen the effect of compounds as a preliminary screening for potential promising SOX9 inhibitor. Nine compounds were selected for further study based on their activity and stability. Compounds from each virtual screen of the protomols were separated in two plates: A & B, given the name accordingly followed by the designated well number of compound given in the two 96 well plates. Four of the chosen nine compounds were in Plate A: A9, E1, F9, & G3; the other five were in Plate B: A4, A9, C1, D3, & F4. For follow up analysis of dose-dependent antiproliferative activity, MDA-MB-231 cells were plated 24 hour prior to treatment with different concentration of inhibitor for 72 hours. The results suggests there is little or no activity of compound D3 and A4 at lower concentration but with increase concentration (7.5 uM-10 uM) there was a 50-100% change in cell viability. Compounds F4, C1, & A9 show that there was a significant change in cell viability causing majority cells died at low concentrations (F4 Compound = 625nm, C1 Compound = 2.5uM, A9 Compound = 5uM). Using the same experimental protocol, we tested selected compounds against non-malignant cells with low expression of SOX9 (HS27 and MCF10a), cancer cells with moderate SOX9 levels (SW480) and cancer cells with high expression of SOX9 (MDA231 and SW620). These results suggest that compounds B-F4 and B-A9 could be potential SOX9 inhibitors.

Figure 3 Non-Malignant Cell vs. Selected Compounds

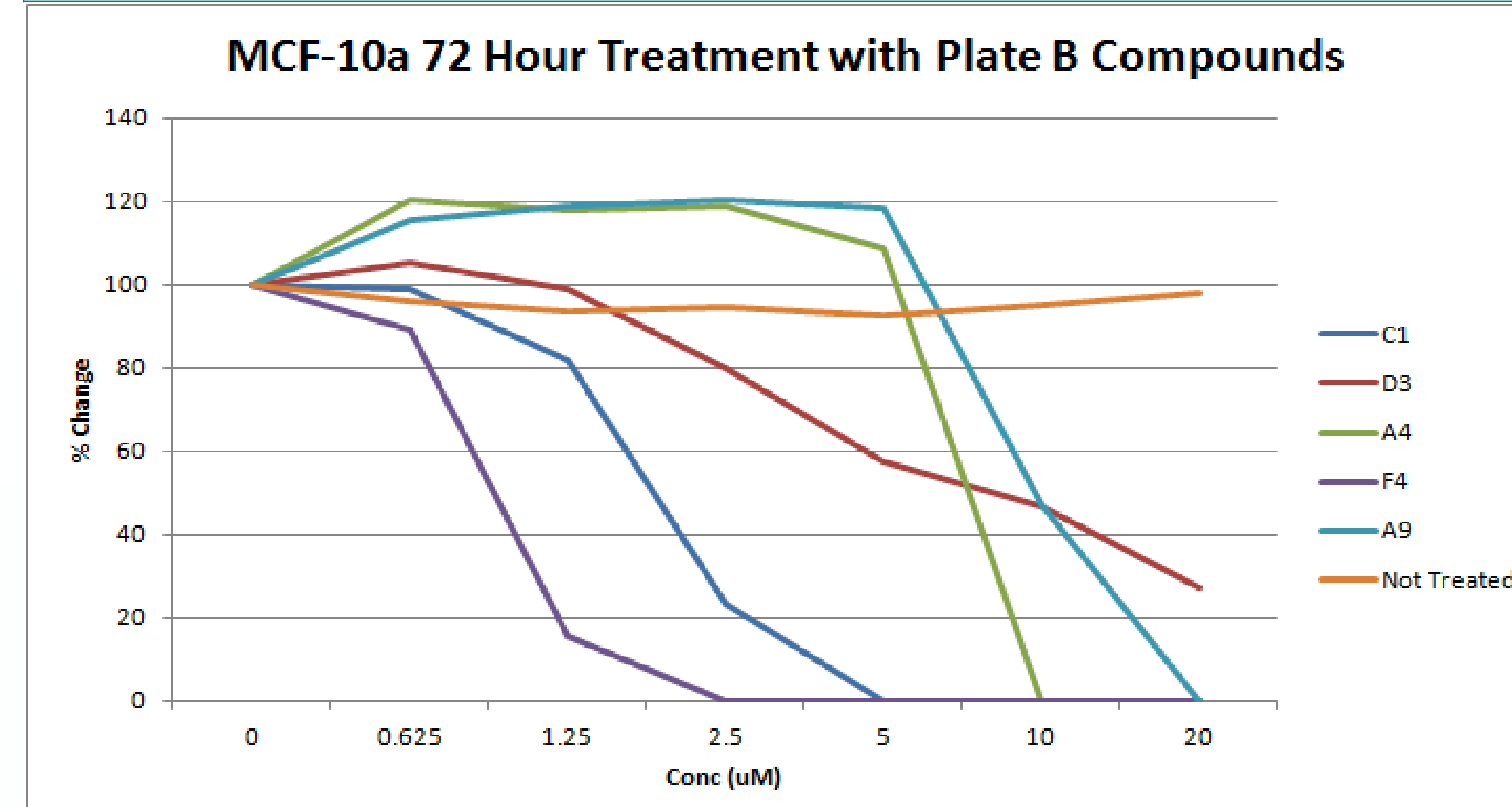


Figure 5: Malignant vs. Non-Malignant Comparison of Compound F4

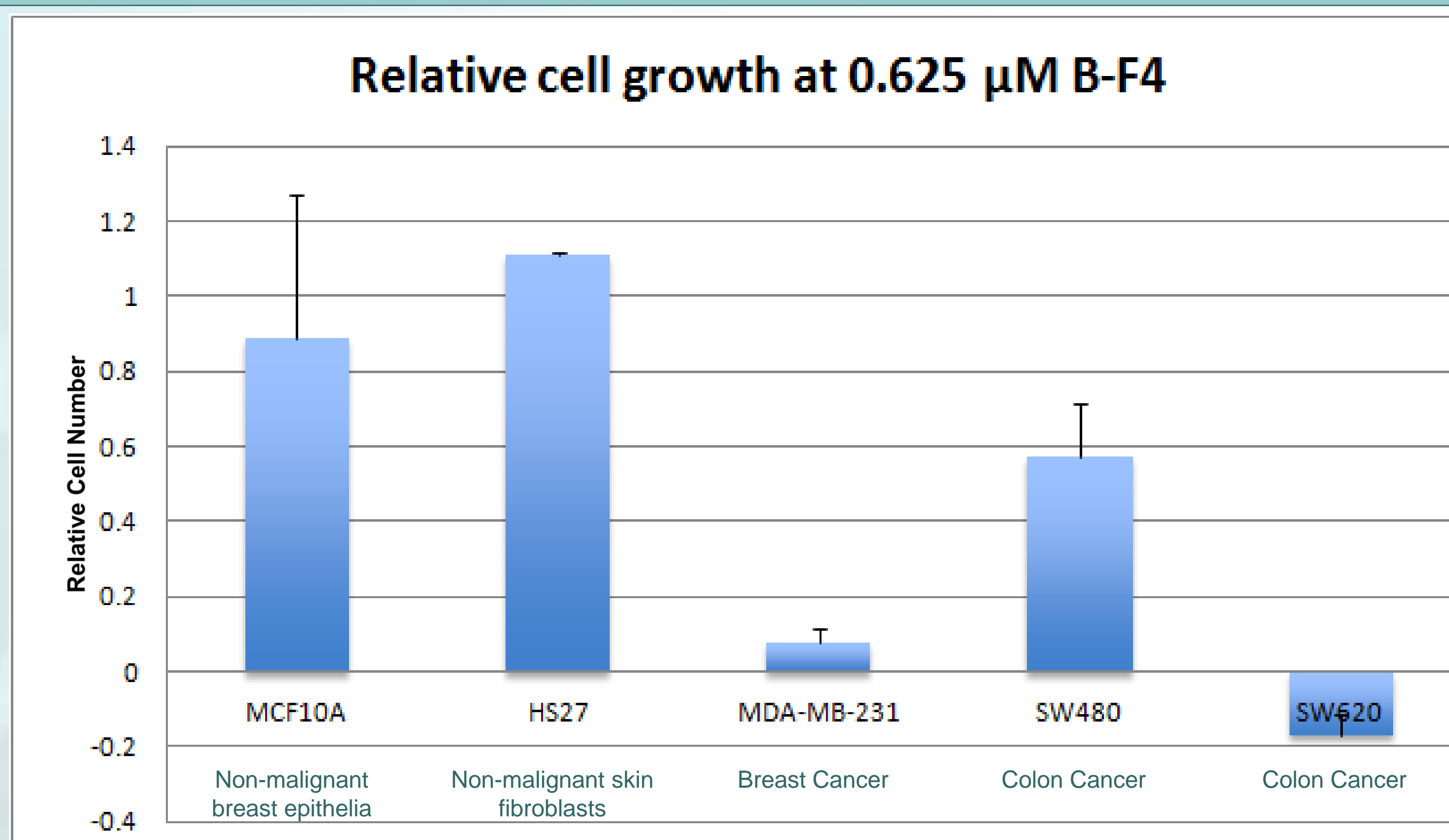


Figure 5: MTT Assay: Compound B-F4 at 0.625 (uM) shows specific antiproliferative activity against malignant cells, MDA-MB231 (breast cancer), SW-620 and SW 480 (colon cancer), whereas as there is no or little effect on non-malignant cells, HS27 (skin fibroblast) and MCF10A (breast epithelial).

References:

- Chakravarty G, Moroz K, Makridakis NM, Lloyd SA, Galvez SE, Canavello PR, Lacey MR, Agrawal K, Mondal D: Prognostic significance of cytoplasmic SOX9 in invasive ductal carcinoma and metastatic breast cancer. *Exp Biol Med* 2011, 236:145-155
- Furumatsu T, Asahara H: Histone Acetylation Influences the Activity of Sox9-related Transcriptional Complex. *Acta Med. Okayama* 2010, Vol 64 #6 pp 351-357
- Jiang SS, Fang WT, Hou YH, Huang SF, Yen BL, Chang JL, et al. Upregulation of SOX9 in lung adenocarcinoma and its involvement in the regulation of cell growth and tumorigenicity. *Clin Cancer Res* 2010;16:4363-73
- Palasingam, P.; Jauch, R.; Ng, C. K.; Kolatkar, P. R. *Journal of molecular biology* 2009, 388, 619.
- Suite 2012: Prime, version 3.1, Schrödinger, LLC, New York, NY, 2012.

Conclusion:

Of 182 compounds identified as potential SOX9 inhibitors, the two most promising compounds from the preliminary screening and analysis are B-A9 & B-F4. Both of these compounds show specific antiproliferative effects on SOX9-expressing cancer cells at relatively low concentrations, whereas they have little or no effect on non-cancerous cells. These compounds have also been found to be very stable at room temperature. Structures of the compounds are not shown here because they have not yet been protected by a patent filing.

Future Directions:

Future studies will attempt to demonstrate that these compounds work by directly inhibiting SOX9. Techniques include: SOX9-driven luciferase reporter assay, electrophoretic mobility shift assay (EMSA), immunohistochemistry, and western blots.



The Anti-glycolytic Small Molecule Inhibitor PFK158 Cooperates with Temozolomide to Induce Cell Death in Melanoma Cells

Adam Morrison^{1,2}, Julie O'Neal³, Jason Chesney³

Departments of Surgery¹, Biochemistry², and Department of Medicine³
University of Louisville School of Medicine

INTRODUCTION

From 1979 to 2009 there has been an 800 percent increase in melanoma among young women and a 400 percent increase among young men. It is estimated that 45,060 new cases of invasive melanoma in men and 31,630 in women will be diagnosed in the US in 2013. Temozolomide (TMZ) is an alkylating agent commonly used in the treatment of melanoma. Response rates to TMZ for metastatic melanoma remain poor, suggesting the need for alternative therapies. The mechanism that imparts TMZ with its therapeutic activity is its ability to methylate or alkylate DNA, which triggers apoptotic cell death. Glutathione (GSH) is involved in prevention and repair of DNA damage. Since we believe that the 6-phospho-2-kinase (PFK158) inhibitor decreases GSH, we hypothesized that the addition of PFK158 to cells treated with TMZ would increase cellular sensitivity to TMZ. Additionally, since melanoma cells are glycolytic, effects of PFK158 may also cooperate with TMZ to promote cell death. PFK158 and TMZ were used in combination on the A375 melanoma cell line. The efficacy of the combination therapy was evaluated using flow cytometry to assess the death of the melanoma cells.

Background

- High glycolytic flux in the presence of oxygen is a common feature of neoplastic cells including melanoma
- PFK 158 is a small molecule inhibitor of glycolysis.

• Preliminary data suggests that PFK158 decreases glutathione and increases reactive oxygen species.

• We hypothesized PFK 158 and TMZ would synergize to kill melanoma cells

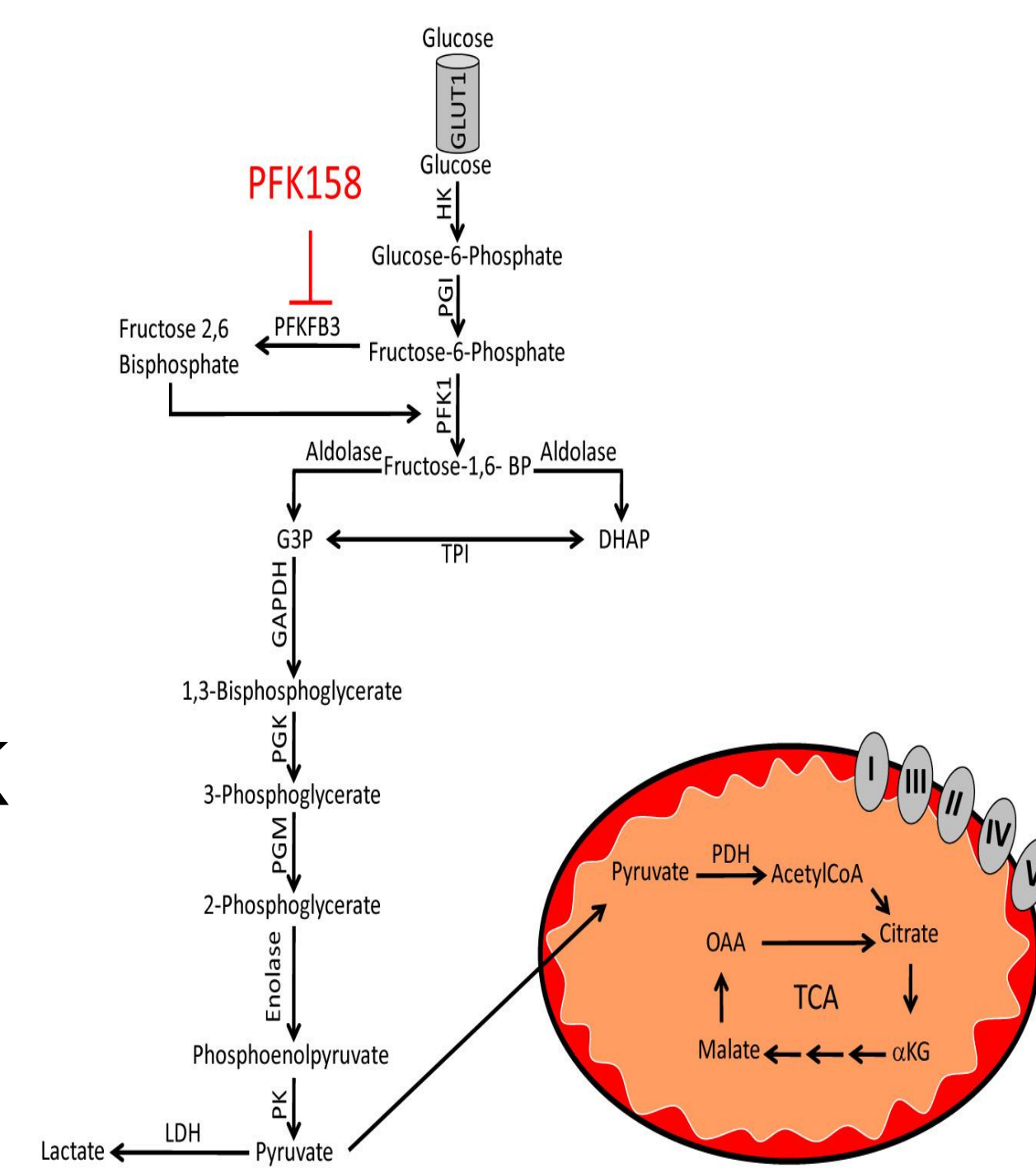


Figure 1. Inhibition of Glycolysis via PFK 158.

RESULTS

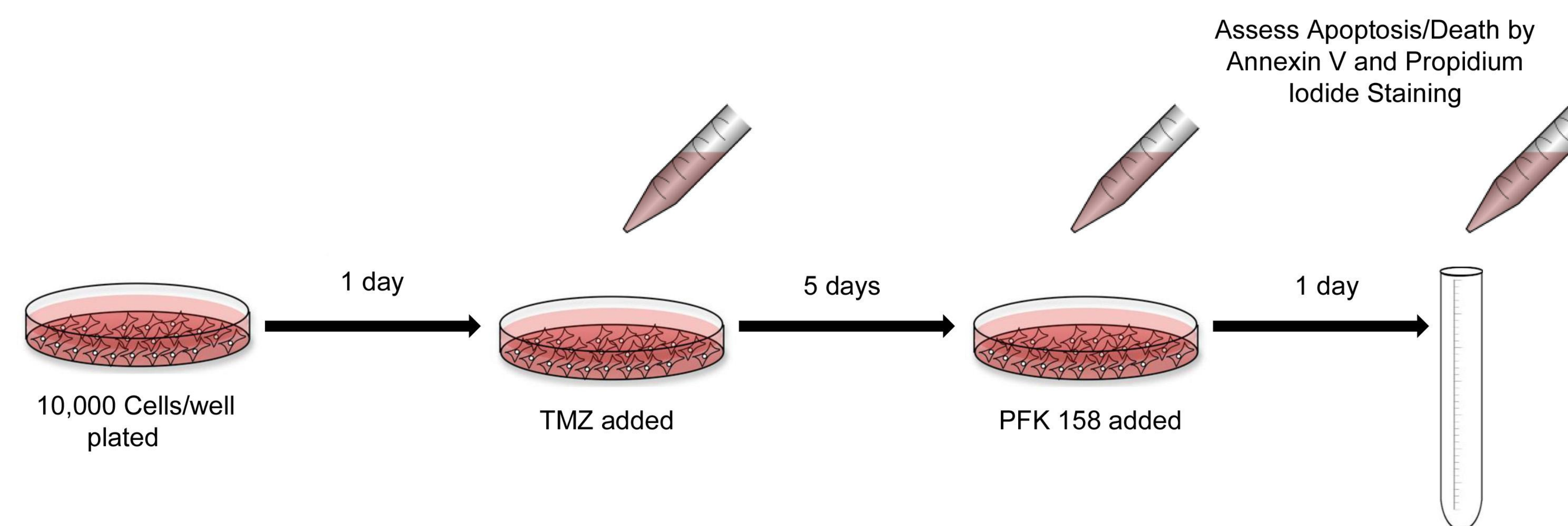


Figure 2. 2,000 A375 melanoma cells were plated. The cells were treated with TMZ 24 hours later. The cells were allowed to incubate for 5 days to allow TMZ to be converted from a pro-drug to its active form. PFK 158 was then added for 24 hours and cells collected for flow cytometry

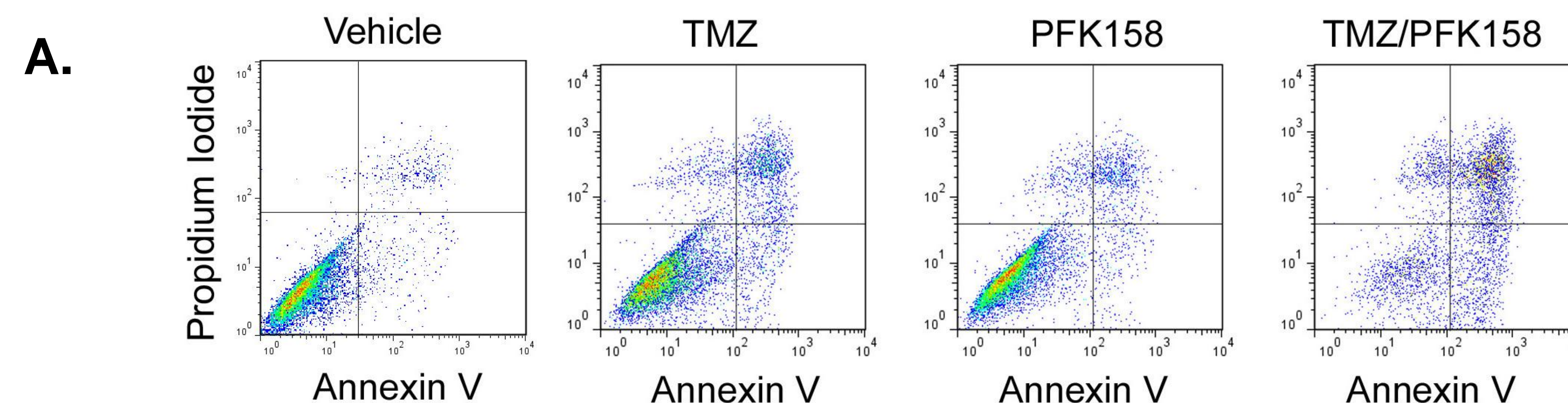


Figure 3A. Flow cytometry data showing cells treated with Vehicle, TMZ, PFK 158, and the combination of PFK 158 and TMZ

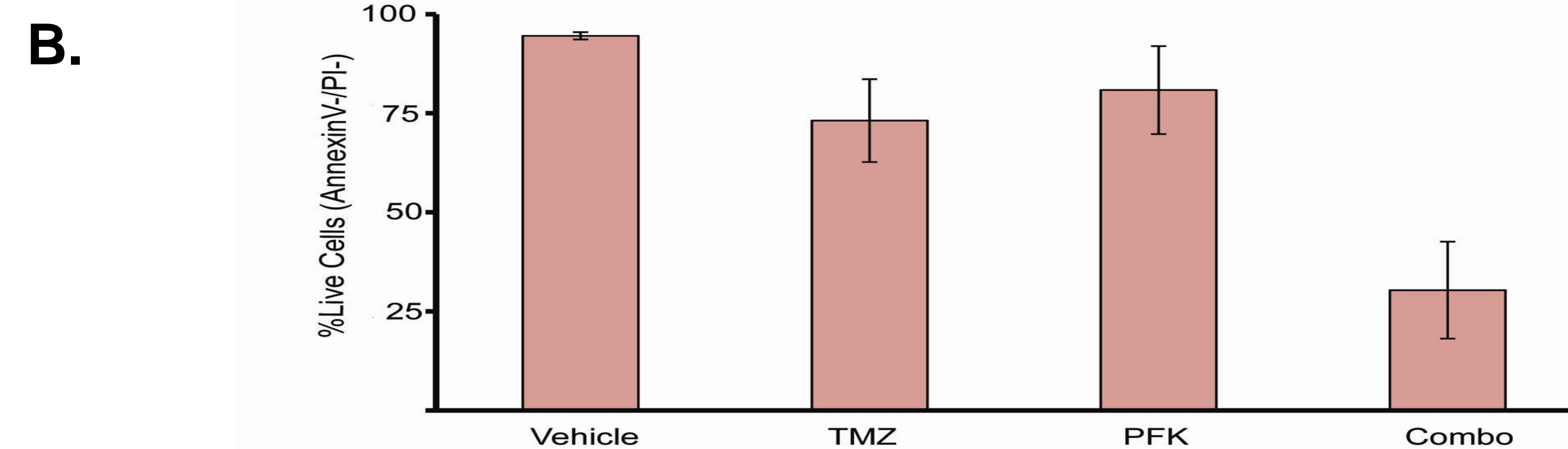


Figure 3B. Quantitated cytometry data showing the percentage of live cells (bottom left quadrant from figure 3A) across the experimental parameters.

METHODS

Cell Culture- A375 cells were cultivated in DMEM with 10% FBS and gentamicin.

Treatment- Cells were grown 2,000 cells/well were plated the following day and were treated with TMZ for 5 days. PFK158 was then added and the cells allowed to incubate for an additional day.

Measuring Cell Death- Cells were trypsinized and collected in FACS tubes. Propidium Iodide and Annexin V were added and incubated for 15 minutes. The cells were analyzed by flow cytometer. 10,000 events were recorded on each sample. Dead cells (PI) and pre-apoptotic cells (Annexin V) were stained by probes allowing the counts to be made.

CONCLUSION

□ The addition of PFK158 to Temozolomide treated cells produces more cell death via apoptosis than TMZ or PFK 158 alone.

□ Future experiments will address the mechanism of additive cell death.

ACKNOWLEDGEMENTS

Supported by grant R25- CA-134283 from the National Cancer Institute



U OF L Sinusoidal endothelial cell-derived extracellular matrix regulates basal and stimulated macrophage activation

Lauren G. Poole, Jenny D. Jokinen, Veronica L. Massey, Juliane I. Beier, and Gavin E. Arteel

Department of Pharmacology and Toxicology, University of Louisville Alcohol Research Center, University of Louisville HSC, Louisville, KY.

ABSTRACT

Background. Fatty liver disease, be it from alcohol (ALD), obesity (NAFLD) or other sources (e.g. viral infection), involves chronic inflammation, although the mechanism(s) are incompletely understood. One potential mechanism contributing to chronic hepatic inflammation is crosstalk between the extracellular matrix (ECM) of hepatic sinusoidal endothelial cells (SEC) and resident macrophages. Here, this hypothesis was tested in vitro using cultured SECs and macrophages. **Methods.** Transformed hepatic sinusoidal endothelial cells (TSECs) were cultured for 72 hours. Culture plates were then washed with a solution that selectively removed the cells, but preserved the ECM. Cultured macrophages (RAW 264.7 cells) were seeded on the matrix and cultured for 24 hours; then stimulated with LPS for 0, 3, 6, 12, or 24 hours (10 or 100 ng/mL). Real time RT-PCR was used to measure mRNA expression of proinflammatory (IL-6, IL-1 β , TNF- α , and iNOS) and anti-inflammatory mediators (IL-10 and TGF- β). **Results.** LPS stimulated production of all mediators by macrophages. With 100 ng/mL LPS, the expression of IL-6, IL-1 β , and IL-10 was attenuated by TSEC ECM, whereas expression of TNF- α , iNOS, and TGF- β increased. Interestingly, the effect of TSEC ECM on the response lower dose LPS (10 ng/ml) tended to be opposite to that observed with the higher dose. Experiments with the integrin inhibitor, CycloRGDfV, indicated that some effects may be mediated via TSEC ECM binding to integrin receptors. **Conclusions.** These data serve as first proof-of-concept that macrophage activation can be modulated by TSEC-derived ECM and identifies a new interaction between these cells that may contribute to inflammatory liver disease.

BACKGROUND

Fatty liver disease, including both ALD and NAFLD, affects more than 30 million people in the United States (1). The diseases include a spectrum of disease states, from simple steatosis, to active inflammation, to advanced fibrosis and cirrhosis (2), but mechanisms of progression are unclear. Importantly, cirrhosis is by far the leading cause of hepatocellular carcinoma (HCC), an almost universally fatal cancer. Here, it is proposed that subtle changes in the hepatic ECM, either in protein composition or amount, caused by a first "hit" can sensitize the liver to a second inflammatory insult.

Previous studies from this group have shown that ECM remodeling, specifically accumulation of the ECM protein fibrin, plays a critical role in the early development of experimental models of both ALD and NAFLD (3, 4). Furthermore, liver injury and inflammation were dramatically blunted by blocking fibrin deposition in these models (3). Taken together, the results of these studies suggest that hepatotoxins may cause an altered ECM profile in the area of the sinusoids and that this altered ECM may be pro-inflammatory. Therefore, the current study was designed to further explore the mechanisms underlying pro-inflammatory effects of altered ECM in the liver.

This study focused on the role of two non-parenchymal hepatic cells that may mediate the effects of ECM on inflammation: sinusoidal endothelial cells and Kupffer cells. Sinusoidal endothelial cells (SECs) line the hepatic sinusoids, where ECM often accumulates in the liver. The accumulation of this ECM, and other ECM components, may be mediated by SECs. However, this hypothesis has never been tested. Kupffer cells, the resident macrophages of the liver, are also well-known to play a key role in liver injury and inflammation through the release of pro-inflammatory cytokines, such as TNF- α (5). In living systems, SECs and Kupffer cells are constantly interacting and communicating, possibly via integrin interaction (6). Therefore, it is hypothesized that SEC-derived matrices directly affect the inflammatory response of macrophages. This study will further understanding of the role of SEC-derived matrices and the effect of these matrices on hepatic macrophage response, which could potentially lead to new therapies.

MATERIALS AND METHODS

Cell culture: Transformed sinusoidal endothelial cells (TSECs) were a generous gift from the laboratory of Dr. Vijay H. Shah (Mayo Clinic and Foundation). TSECs were maintained in DMEM (Sigma) with 5% fetal bovine serum (FBS), 1% antibiotic/antimycotic, and endothelial cell growth supplement (ScienCell) and incubated in a humidified 5% CO₂ incubator at 37 °C. Cells were passaged at confluency every 3-4 days using a solution of 0.05% trypsin with EDTA and split by adding 100 μ L of the trypsinized monolayer to 10 mL of media. RAW 264.7 cells (ATCC) were maintained in DMEM (Sigma) with 5% FBS and 1% antibiotic/antimycotic and incubated in a humidified 5% CO₂ incubator at 37 °C. Cells were passaged every 3-4 days by gently scraping the side of the culture flask using a cell scraper (no trypsin) and split by adding 1 mL detached cells to 9 mL of media.

Treatment of cells: (Scheme 1) TSECs (passage 5-6) were seeded on a 12-well plate (Nunc) at a density of 50,000 cells per well in 1.0 mL of media. To control for the effect of TSEC-derived ECM, some wells (control wells) were treated in parallel, but devoid of cells. Cells were incubated for 72 h, then were washed and treated with a solution containing 0.25 M ammonium hydroxide and 1 mM EDTA to selectively remove the cells and preserve the ECM. After three washes, the ECM produced by the TSECs was used as a substratum for culturing RAW 264.7 cells (7,8). RAW 264.7 cells (passage 4-14) were seeded at a density of 150,000 cells per well in 1.0 mL of media on the preserved TSEC ECM or in control wells and incubated for 24 hours. Then, cells were exposed to LPS (100 ng/mL) \pm CycloRGDfV (10 μ M) for an additional 3, 6, 12, or 24 hour incubation period. Upon termination, supernatant was removed and stabilized with 10 μ L aprotinin (1 mg/mL) and stored at -80 °C for further analysis. 0.25 mL RNA STAT was added to each well to lyse the cells and to prepare the lysate for RNA isolation.

RNA isolation and real time RT-PCR: Total RNA was extracted from RAW 264.7 cells by a guanidium thiocyanate-based method (RNA STAT 60 Tel-Test, Ambion, Austin, TX). RNA concentrations were determined spectrophotometrically and 1 μ g total RNA was reverse transcribed using a kit (Quanta Biosciences, Gaithersburg, MD). Real time PCR was performed using the ABI StepOne Plus Software and PerfeCta qPCR FastMix (Quanta Biosciences, Gaithersburg, MD). The comparative CT method was used to determine fold changes in mRNA expression compared to control.

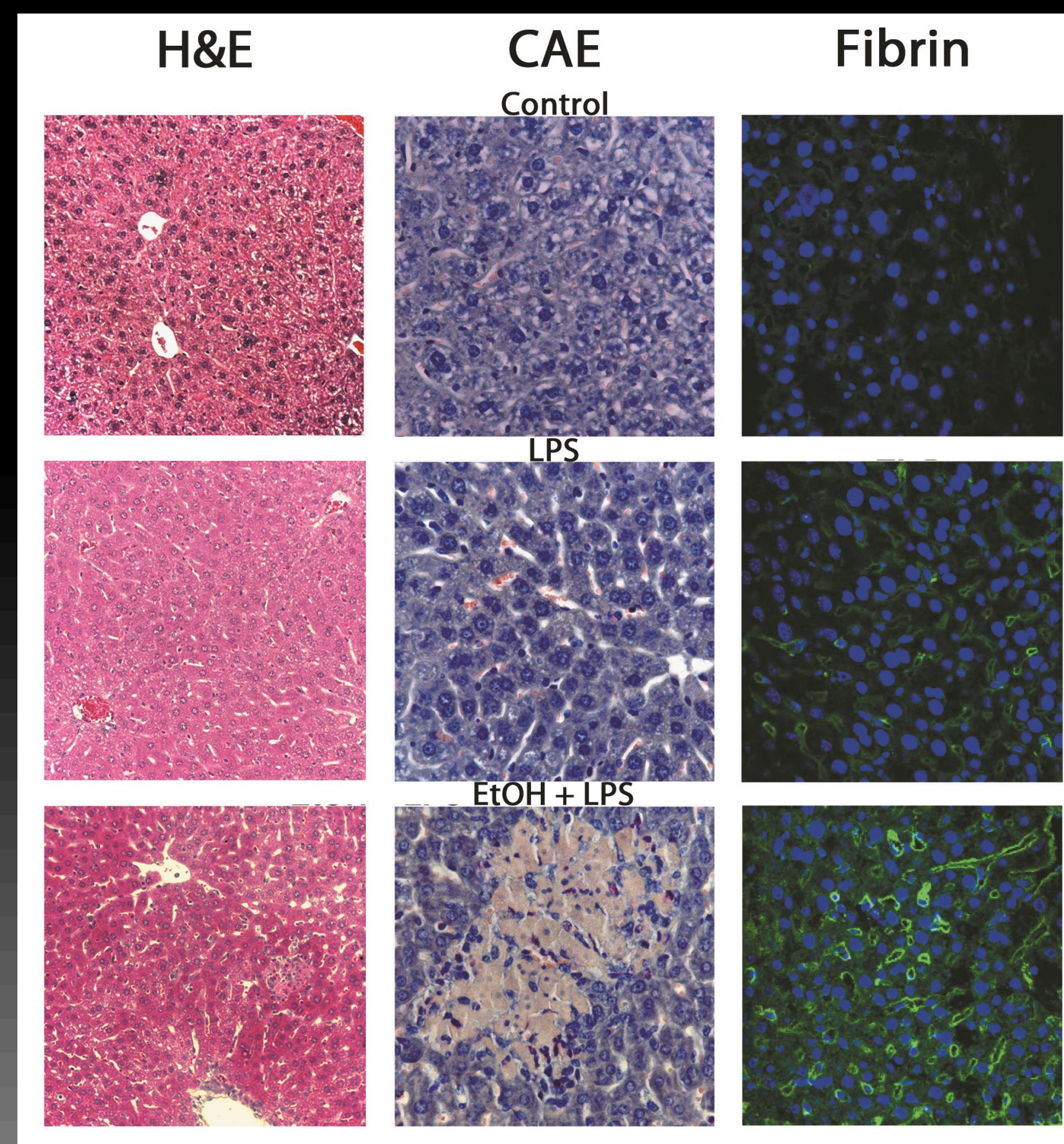
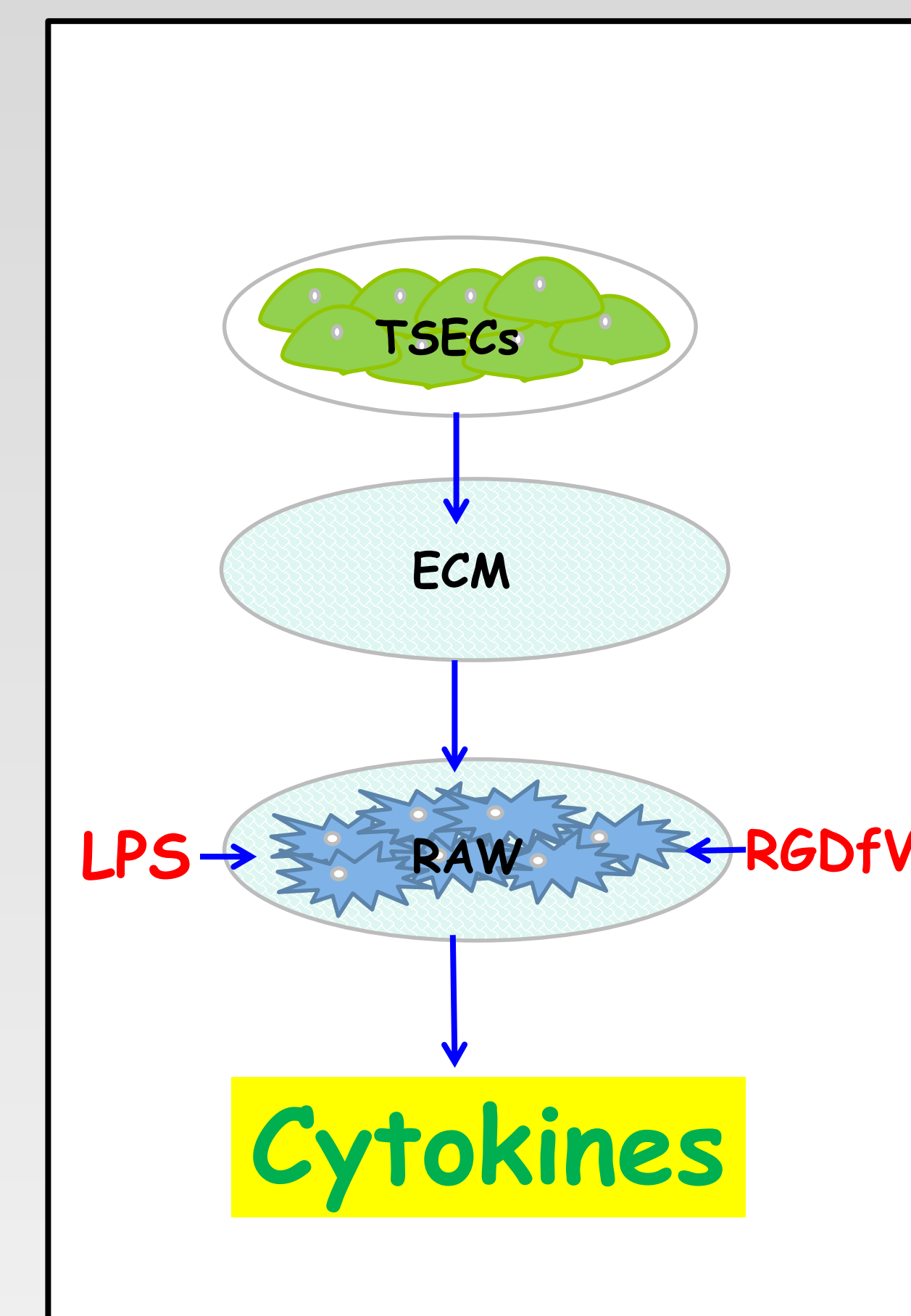


Figure 1: Fibrin deposition correlates with liver damage and neutrophil infiltration. Data are from Beier et al. (2009). Representative photomicrographs depicting hematoxylin & eosin (H&E; left column), chloracetate-esterase staining (CAE; center column), and immunofluorescent detection of hepatic fibrin (right column) 24 h after LPS are shown.

LPS alone caused no gross morphological changes in the liver, but increased the number of infiltrating neutrophils and fibrin deposition compared to controls. The combination of LPS and ethanol caused macroscopically detectable necroinflammatory foci indicative of liver damage. Ethanol pre-exposure enhanced the effects of LPS on both neutrophil infiltration and fibrin deposition.



Scheme 1: TSECs were seeded on a 12-well plate and incubated for 72 hours. After incubation, TSECs were washed and treated to selectively remove the cells and preserve the ECM. The extracellular matrix deposited by the TSECs was used as a substratum for the RAW 264.7 cells which were incubated for 24 hours. Then, cells were treated with LPS (10 or 100 ng/mL) \pm CycloRGDfV (10 μ M) for an additional 24 hour incubation period.

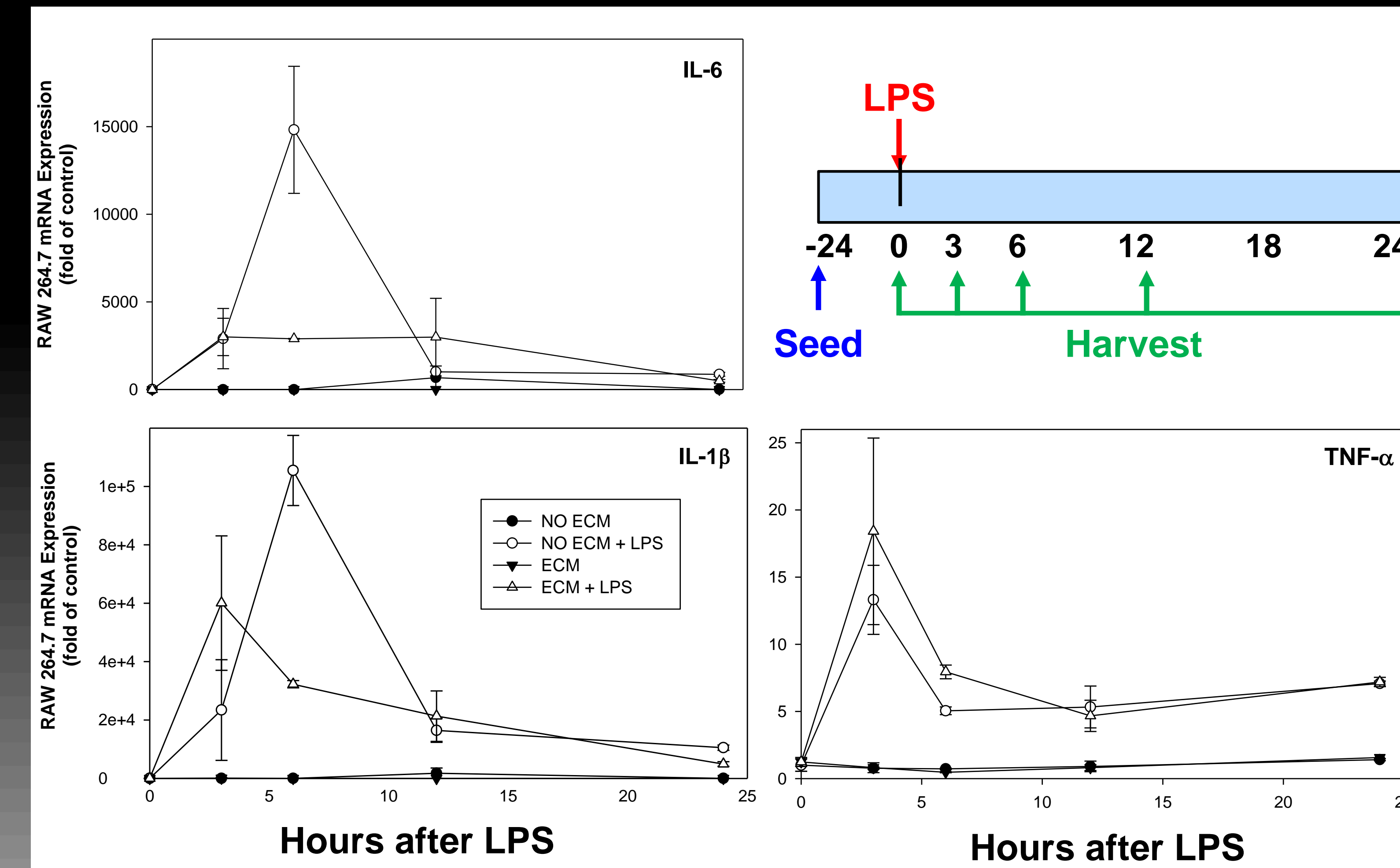


Figure 2: TSEC-derived ECM attenuates expression of proinflammatory cytokines by RAW 264.7 cells. RAW 264.7 macrophages and TSECs were cultured and treated as described in *Materials and Methods*. Macrophages were cultured on TSEC-derived ECM or in control wells. Cells were treated with 100 ng/mL LPS and harvested at 0, 3, 6, 12, and 24 hours. Real-time RT-PCR was used to determine mRNA expression of inflammatory mediators IL-6, IL-1 β , TNF- α . Data are means \pm SEM and are expressed as fold of control.

LPS induced expression of all mediators. In the absence of TSEC-derived ECM, cytokine expression peaked at 6 hours for IL-6 and IL-1 β and at 3 hours for TNF- α . The same peaks occurred in the presence of TSEC-derived ECM with the exception if IL-1 β expression, which occurred at 3 hours. At 6 hours, the presence of TSEC-derived ECM attenuated expression of IL-6 and IL-1 β , but enhanced TNF- α expression.

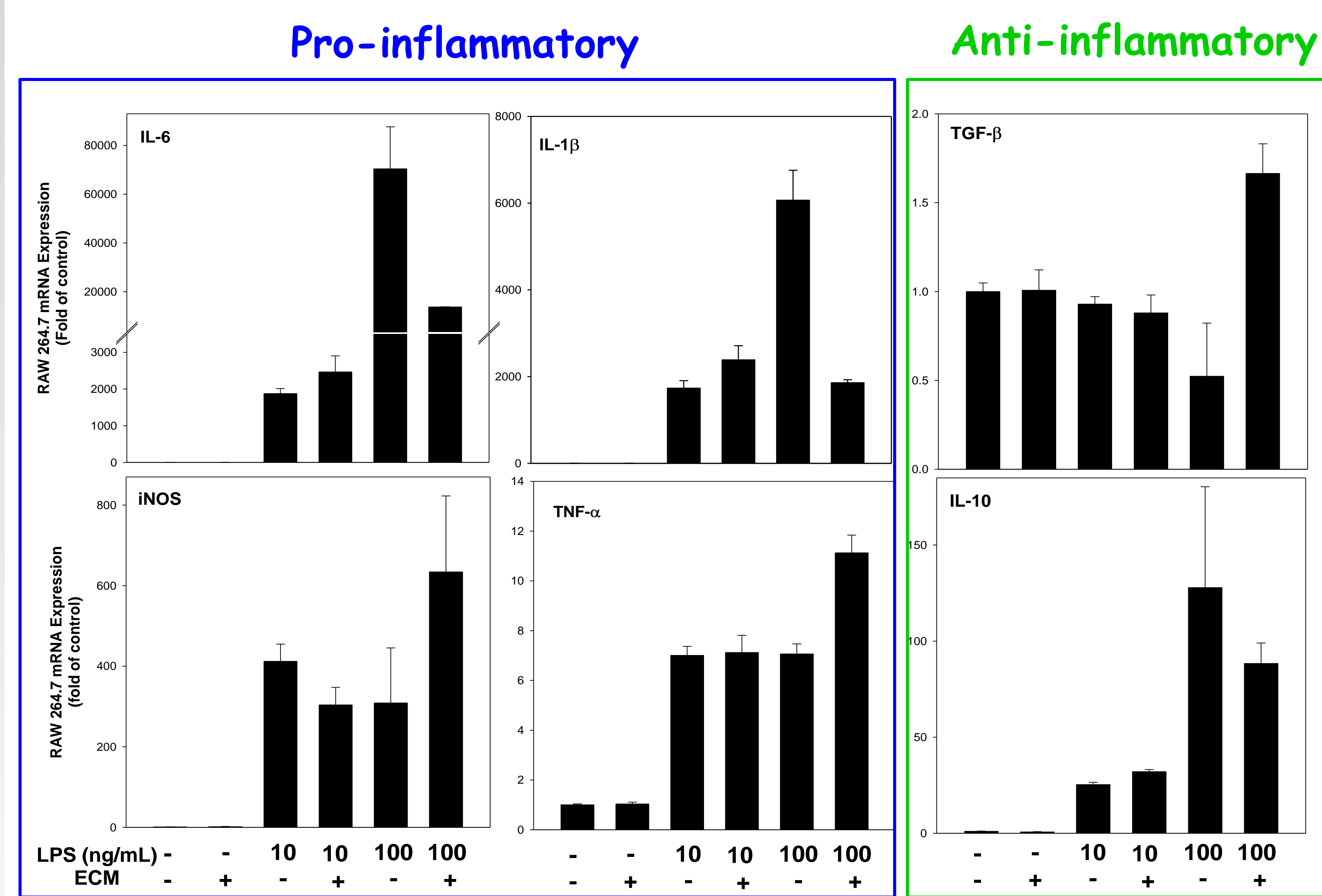


Figure 3: Effect of TSEC-derived ECM on production of pro-inflammatory cytokines by RAW 264.7 cells is dependent on LPS dosage. TSECs and RAW 264.7 cells were cultured and treated as described in *Materials and Methods* for 6 hours with 0, 10, or 100 ng/mL LPS. Real-time RT-PCR was used to determine mRNA expression of inflammatory mediators IL-6, IL-1 β , iNOS, TNF- α , TGF- β , and IL-10. Data are means \pm SEM and are expressed as fold of control.

At 10 ng/mL LPS, the presence of TSEC-derived ECM increased expression of inflammatory mediators IL-6 and IL-1 β , decreased expression of iNOS, and had no effect on TNF- α expression. At 100 ng/mL LPS, the presence of TSEC-derived ECM decreased IL-6 and IL-1 β expression and increased iNOS and TNF- α expression. Anti-inflammatory mediator TGF- β expression was unaffected by TSEC-derived ECM at 10 ng/mL LPS, while IL-10 expression as slightly enhanced. At 100 ng/mL LPS, TGF- β expression increased in the presence of TSEC-derived ECM, while IL-10 expression decreased.

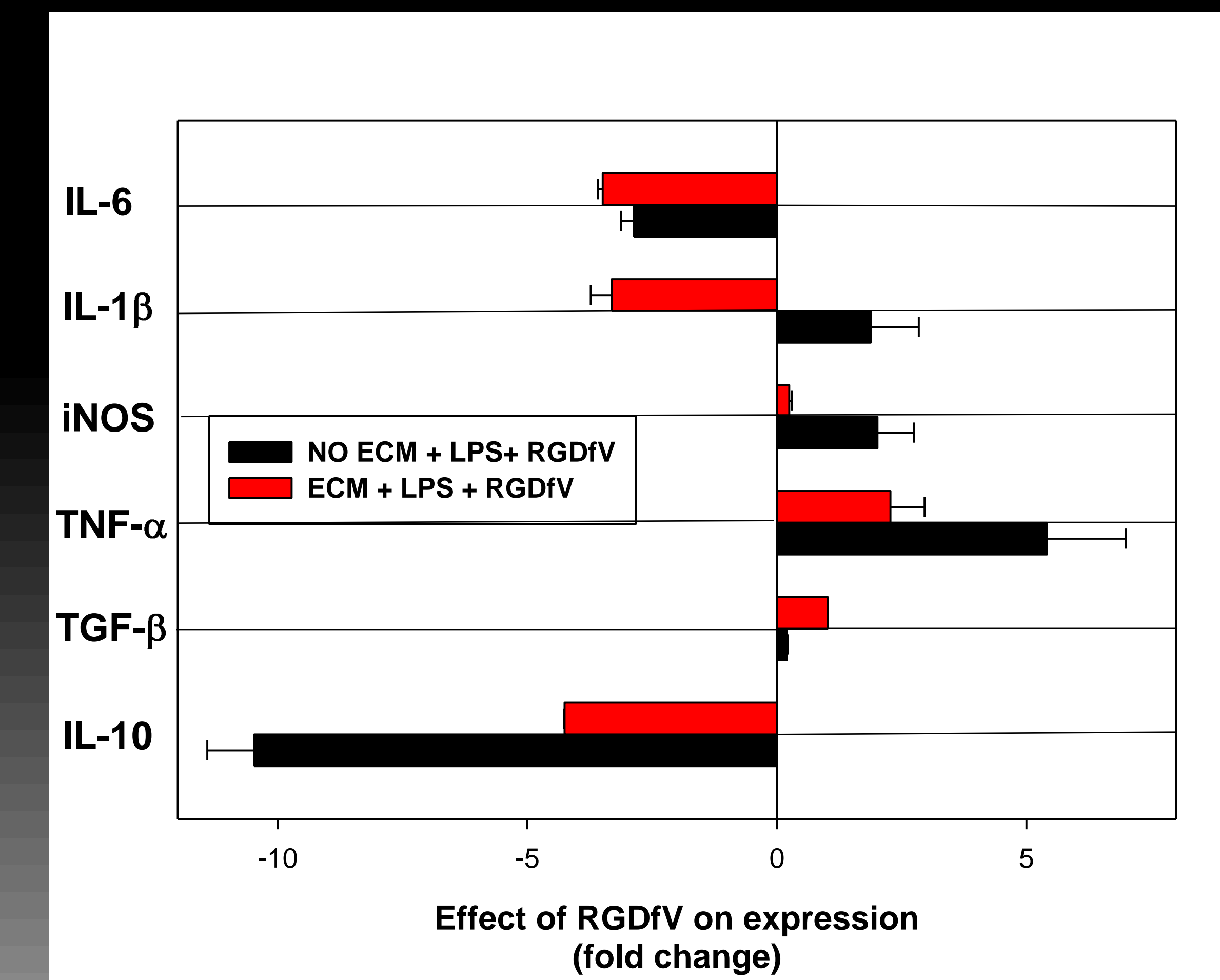
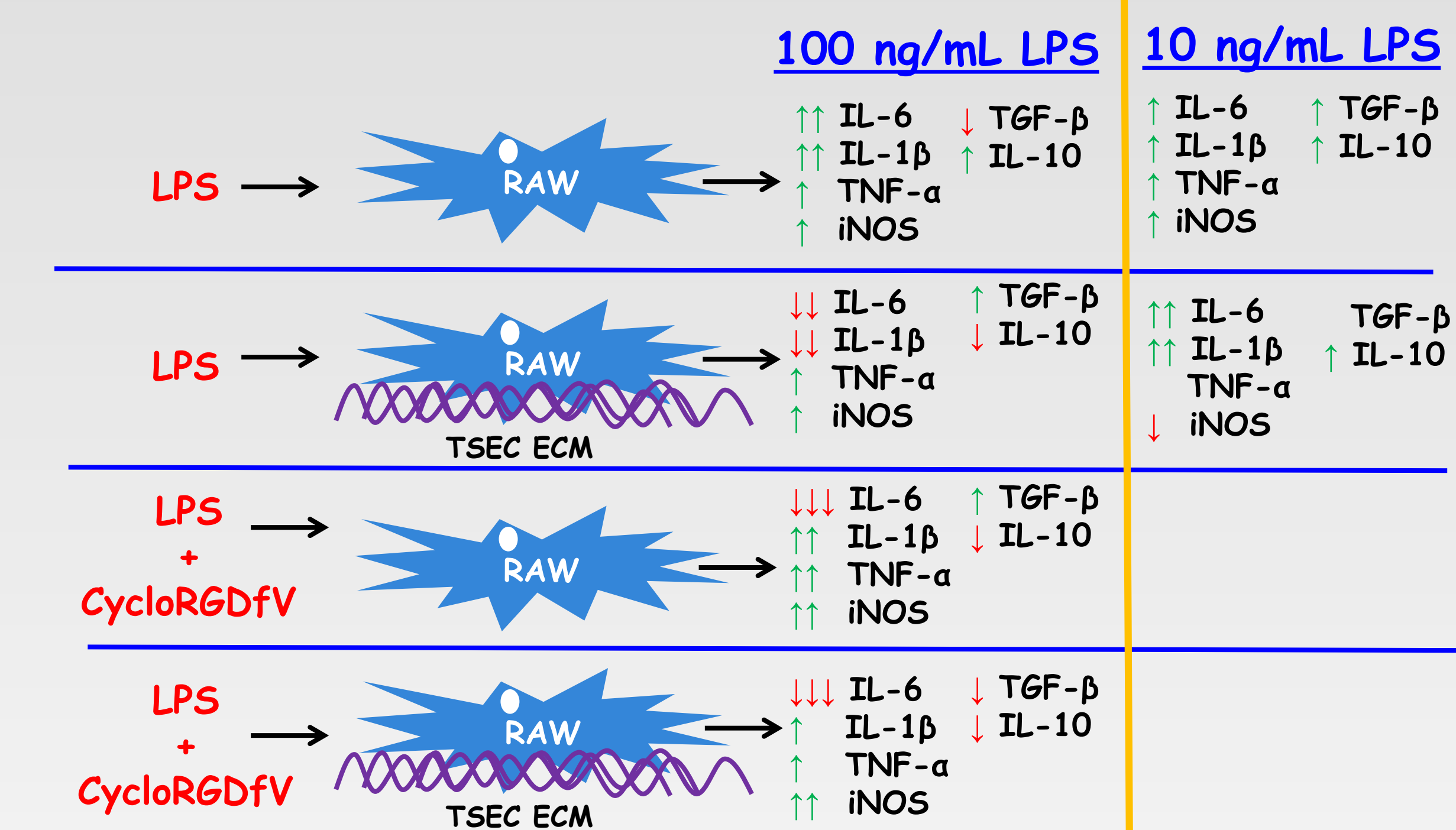


Figure 3: Effect of CycloRGDFV on inflammatory mediator production by RAW 264.7 cells in the presence or absence of TSEC-derived ECM. Cells were treated with LPS (100 ng/mL) \pm CycloRGDFV (10 μ M) in the presence or absence of TSEC-derived ECM as described in *Materials and Methods*. Data are means \pm SEM and are expressed as fold change from LPS alone \pm TSEC-derived ECM.

CycloRGDFV, in the absence of ECM, decreased expression of IL-1 and IL-10, but increased expression of IL-1 β , iNOS, TNF- α , and TGF- β . In the presence of TSEC-derived ECM, CycloRGDFV decreased expression of IL-6, IL-1 β , and IL-10, but enhanced iNOS, TNF- α , and TGF- β expression.

SUMMARY

- At 6 hours, macrophage response to 100 ng/mL LPS in the presence of TSEC-derived ECM was attenuated in terms if IL-6, IL-1 β , and IL-10 expression, whereas iNOS, TNF- α , and TGF- β expression was enhanced.
- 10 ng/mL LPS tended to have the opposite effect on inflammatory mediator expression.
- The effect of CycloRGDFV suggests that some of these effects may be mediated by integrin interactions.
- Macrophage activation can be modulated by ECM produced by TSECs.
- Interaction between SECs and macrophages may contribute to inflammatory liver disease.



REFERENCES

- American Liver Foundation. Liver Awareness Month 2010. 2010.
- Day CP. Non-alcoholic fatty liver disease: current concepts and management strategies. Clin Med 2006 Jan;6(1):19-25.
- Beier JI, Luyendyk JP, Guo L, von Montfort C, Staunton DE, Arteel GE. Fibrin accumulation plays a critical role in the sensitization to lipopolysaccharide-induced liver injury caused by ethanol in mice. Hepatology 2009 Jan 23;49(5):1545-1553.
- Tan M, Schmidt RH, Beier JI, Watson WH, Zhong H, States JC, et al. Chronic subhepatoxic exposure to arsenic enhances hepatic injury caused by high fat diet in mice. Toxicol Appl Pharmacol 2011 Dec 15;257(3):356-364.
- Arteel GE. Oxidants and antioxidants in alcohol-induced liver disease. Gastroenterology 2003 Mar;124(3):778-790.
- Massey VL, Arteel GE. Acute alcohol-induced liver injury. Frontiers in Physiology 2012;3:1-8.
- Brown LA, Ritzenthaler JD, Guidot DM, Roman J. Alveolar type II cells from ethanol-fed rats produce a fibronectin-enriched extracellular matrix that promotes monocyte activation. Alcohol 2007 Aug;41(5):317-324.
- Dunsmore SE, Lee YC, Martinez-Williams C, Ramelis DE. Synthesis of fibronectin and laminin by type II pulmonary epithelial cells. Am J Physiol 1996 Feb 1;270(2):L219-L223.

Grant support: R25-CA-134283 (NCI) is gratefully acknowledged